Irregular Wave Setup and Runup on Cobble Beaches and Revetments

by

Francisco J. de los Santos and Nobuhisa Kobayashi

RESEARCH REPORT NO. CACR-05-06
July, 2005

ABSTRACT

A time-averaged probabilistic model is developed to predict irregular wave runup statistics on permeable slopes such as cobble beaches and revetments. The cross-shore variations of the mean and standard deviation of the free surface elevation and horizontal fluid velocities above and inside a porous layer are predicted using the time-averaged continuity, momentum and energy equations. The mean and standard deviation of the shoreline elevation measured by a runup wire are estimated from the predicted mean and standard deviation of the free surface elevation. The wave runup height above the mean water level including wave setup is assumed to be given by the Rayleigh distribution. The wave reflection coefficient is estimated from the wave energy flux remaining at the still water shoreline. This computationally efficient model is shown to be in fair agreement with 57 tests conducted on 1/5 and 1/2 permeable slopes situated inside surf zones on impermeable gentle slopes.

The numerical model is shown to predict the cross-shore variations of the mean and standard deviation of the measured free surface elevation and horizontal velocity fairly accurately when the breaker ratio parameter γ is calibrated for some of the 1/2 slope tests. The numerical model predicts the mean and standard deviation of the measured shoreline oscillations reasonably well except that the mean is overpredicted for some of the 1/2 slope tests. Nevertheless, the numerical model predicts the significant and 2% runup heights within the error of about 20%. This accuracy is similar to the accuracy of an available empirical formula based on the known wave conditions at the toe of the permeable slope. The advantage of this numerical model is that it can predict the irregular wave transformation on a beach of arbitrary profile. Furthermore, the numerical model may be applied to gentler permeable slopes for which the effect of wave setup is not negligible. This numerical model is computationally efficient and easy to use because no numerical difficulty has been experienced in the region of very small water depth.

ACKNOWLEDGEMENTS

This study was partially supported by the U.S. Army Corps of Engineers, Coastal and Hydraulics Laboratory under Contract Number DACW42-03-C-0024. The first author was supported by a Scholarship from the Spanish Ministry of Education, F.P.U. AP20024082. The authors would like to thank Peter G. Kearney for providing the data of his 1/2 permeable slope experiments and Leslie Elizabeth Meigs for her assistance in the 1/5 permeable slope experiments. The first author would like to thank his advisor, Prof. Miguel A. Losada, for all the encouragement and support during his Ph.D. study at the University of Granada, Spain.

TABLE OF CONTENTS

LIST OF FIGURES

LIST OF TABLES

CHAPTER 1 INTRODUCTION

The prediction of irregular wave runup is necessary in determining the crest height of a coastal structure and the landward limit of wave action on a beach. A large number of studies were performed to understand the swash dynamics and predict wave runup for given slope and offshore wave characteristics as reviewed by Kobayashi (1999). The prediction of wave runup was initially based on experiments and empirical formulas because of the complexity involved in wave breaking and runup. Time-dependent numerical models for shallow-water waves were developed to predict regular wave runup (Kobayashi et al. 1987), irregular wave runup on a rough impermeable slope (Kobayashi et al. 1990), and irregular wave runup on a permeable slope (Wurjanto and Kobayashi, 1993). These models are one-dimensional in the cross-shore direction and do not predict the vertical variations of fluid velocities. Vertically two-dimensional models were also developed to predict plunging waves on an impermeable slope (van der Meer et al. 1992) and regular wave interaction with a steep porous structure (Liu et al. 1999). These numerical models predict the detailed temporal and

spatial variations of the free surface elevation and fluid velocities which are needed to understand the complicated hydrodynamics.

For practical applications, the time-dependent models for wave runup have not been applied routinely perhaps because these models require significant computational efforts and experience to run computer programs and obtain quantities of practical importance. On the other hand, empirical formulas for irregular wave runup on coastal structures have been improved to account for various factors (van der Meer and Janssen 1995; van Gent 2001) but are not versatile enough to deal with various combinations of different beaches and structures. These empirical formulas require the input of the representative height and period of incident waves at the toe of the structure which is normally located inside the surf zone during a severe storm. Consequently, a wave model will be necessary to predict the wave transformation from offshore to the toe of the structure.

Irregular wave breaking and wave setup on an impermeable beach of arbitrary profile are generally predicted using numerical models such as that of Battjes and Stive (1985) based on time-averaged momentum and energy equations. Their time-averaged model predicts only the mean and standard deviation of the free surface elevation but is widely used because of its computational efficiency. In this study, the time-averaged model of Battjes and Stive (1985) is extended landward to a permeable slope such as a revetment and a cobble beach. The extended wave propagation model is combined with a probabilistic wave runup model to predict the runup heights of practical importance such as the significant and 2% runup heights. Furthermore, this time-averaged probabilistic model predicts the cross-shore variations of the mean and standard deviation of the free surface elevation and horizontal fluid velocities above and inside the permeable layer.

In the following, the time-averaged probabilistic model is presented first. The laboratory experiments using 1/5 and 1/2 permeable slopes are described second. The

developed model is compared with 57 tests in the two experiments and used to examine the permeability effects on the wave motion on the slope and the sensitivity of the model to the roller effect, the breaker ratio parameter and the bottom friction factor. Finally, the findings of this study are summarized.

It is noted that the results in this report will be presented concisely by de los Santos, Kobayashi, Meigs and Losada (2005) and Kobayashi, de los Santos and Kearney (2005).

CHAPTER 2 NUMERICAL MODEL

The numerical model based on the time-averaged continuity, momentum and energy equations is presented first in this chapter. The effects of bottom friction and the presence of a roller on the cross-shore momentum and energy equations are included. The formula for the energy dissipation rate due to wave breaking developed by Battjes & Stive (1985) is modified to include the effect of a relative steep slope to allow situations where the energy dissipation is more concentrated locally. Furthermore, an extra energy dissipation term is included to account for the flow resistance inside the porous layer. Finally, a probabilistic model for irregular wave runup is developed using the computed mean and standard deviation of the free surface elevation η on the permeable slope.

2.1 TIME-AVERAGED WAVE MODEL

The problem examined here is depicted in Fig. 2-1 where alongshore uniformity and normally incident waves are assumed. The cross-shore coordinate x is positive onshore. The vertical coordinate z is positive upward with $z = 0$ at the still water level (SWL). The upper

and lower boundaries of the permeable stone layer are located at $z = z_b$ and z_p, respectively, where the lower boundary is assumed to be impermeable. The beach in front of the permeable slope is assumed to be impermeable and $z_b = z_p$ on the beach. The instantaneous water depth and free surface elevation are denoted by h and η, respectively, and $h = (\eta - z_b)$. The horizontal fluid velocity u is the depth-averaged velocity. The still water depth d_t at the toe of the permeable slope is located inside the surf zone on the beach in the experiments in this study.

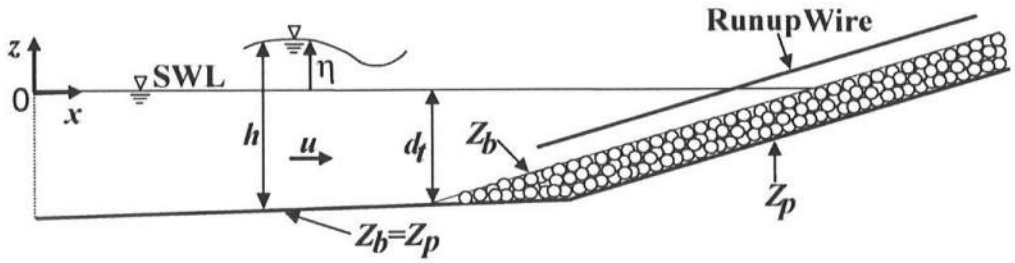

Fig. 2-1: Time averaged model for wave propagation on permeable slope.

The time-averaged continuity, momentum and energy equations used here are those given by Kobayashi et al. (2005) for the prediction of irregular breaking wave transmission over a submerged porous breakwater together with the roller effect discussed by Kobayashi et al. (2005) for sand suspension. These equations are summarized in the following. The time-averaged momentum and energy equations are expressed as

$$\frac{dS_{xx}}{dx} = -\rho g \bar{h} \frac{d\bar{\eta}}{dx} - \tau_b \quad ; \quad \frac{dF}{dx} = -D_B - D_f - D_r \tag{1}$$

where S_{xx} = cross-shore radiation stress; ρ = fluid density; g = gravitational acceleration; $\bar{h}$ = mean water depth with the overbar denoting time averaging; $\bar{\eta}$ = wave setup or setdown; τ_b = time-averaged bottom shear stress; F = wave energy flux per unit width; and D_B, D_f

and D_r = time-averaged energy dissipation rate per unit horizontal area due to wave breaking, bottom friction, and porous flow resistance, respectively.

Linear wave theory for onshore progressive waves is used to estimate S_{xx} and F where the root-mean-square wave height H_{rms} is defined as $H_{\text{rms}} = \sqrt{8}\ \sigma_\eta$ with σ_η = standard deviation of η (Battjes and Stive 1985).

$$S_{xx} = \rho g \sigma_\eta^2 \left(2n - 0.5\right) + \rho C_p q_r \quad ; \quad F = \rho g C_g \sigma_\eta^2 \tag{2}$$

where $n = C_g / C_p$ with C_g and C_p = group velocity and phase velocity in the mean water depth $\bar{h}$ corresponding to the spectral peak period T_p of incident waves, and q_r is the volume flux due to the roller on the steep front of a breaking wave.

The roller effect has been represented by its area or energy (Svendsen 1984) but the roller volume flux is used here because the roller effect is the most apparent in the increase of undertow current. The term $\rho C_p q_r$ in S_{xx} is the roller momentum flux due to the roller propagating with the speed of C_p and causes the landward shift of $\bar{\eta}$ in the breaker zone (Kobayashi et al. 2005). The dissipated wave energy is converted to the roller energy which is assumed to be governed by (Stive and DeVriend 1994)

$$\frac{d}{dx}\left(\rho C_p^2 q_r\right) = D_B - \rho g \beta_r q_r \tag{3}$$

where the roller dissipation rate, $\rho g \beta_r q_r$, is assumed to equal the rate of work to maintain the roller on the wave-front slope β_r of order 0.1 (Deigaard 1993).

The bottom shear stress τ_b and the corresponding dissipation rate D_f are expressed using the formulas based on the quadratic drag force based on the horizontal velocity u. The mean and standard deviation of u are denoted by $\bar{u}$ and σ_u, respectively. The Gaussian

distribution of u and the equivalency of the time and probabilistic averaging are assumed to express τ_b and D_f in terms of $\bar{u}$ and σ_u

$$\tau_b = \frac{1}{2}\rho f_b \sigma_u^2 G_2(u_*) \quad ; \quad D_f = \frac{1}{2}\rho f_b \sigma_u^3 G_3(u_*) \quad ; \quad u_* = \frac{\bar{u}}{\sigma_u} \tag{4}$$

where f_b = bottom friction factor which is taken as $f_b = 0$ on the beach and $f_b = 0.01$ on the stone slope (Kobayashi et al. 2005). The analytical functions $G_2(r)$ and $G_3(r)$ for the arbitrary variable r are given by Kobayashi et al. (2005) and can be approximated as $G_2 \simeq 1.64r$ and $G_3 \simeq (1.6 + 2.6r^2)$ for $|r| < 1$.

The standard deviation σ_u is estimated using the relationship between σ_u and σ_η based on linear shallow-water wave theory (Kobayashi et al. 1998)

$$\sigma_u = \sigma_* \left(g\bar{h}\right)^{0.5} \quad ; \quad \sigma_* = \sigma_\eta / \bar{h} \tag{5}$$

The mean $\bar{u}$ is estimated using the time-averaged, vertically-integrated continuity equation $\left(\sigma_u \sigma_\eta + \bar{u}\bar{h} + \bar{v}h_p + q_r\right) = 0$ with the condition of no net landward water flux. In this equation, $\sigma_u \sigma_\eta$ is the onshore flux due to linear shallow-water waves (Kobayashi et al. 1998), $\bar{u}\bar{h}$ is the offshore flux due to the return current $\bar{u}$, q_r is the volume flux due to the roller of a breaking wave, and $\bar{v}h_p$ is the water flux inside the permeable layer of vertical height h_p due to the time-averaged horizontal discharge velocity $\bar{v}$. Substitution of Eq. (5) into the continuity equation yields

$$\bar{u} = -\left[\sigma_*^2 \sqrt{g\bar{h}} + \bar{v}h_p / \bar{h} + q_r / \bar{h}\right] \quad ; \quad h_p = z_b - z_p \tag{6}$$

where $h_p = 0$ on the impermeable beach.

The energy dissipation rate D_r in Eq. (1) is estimated using the formula by Wurjanto and Kobayashi (1993) based on the discharge velocity v whose probability distribution is assumed to be Gaussian

$$D_r = \rho h_p \left[\alpha \sigma_v^2 \left(1 + v_*^2\right) + \beta \sigma_v^3 G_3\left(v_*\right) \right] \quad ; \quad v_* = \frac{\bar{v}}{\sigma_v} \tag{7}$$

where σ_v = standard deviation of v; G_3 = same function as in Eq. (4) except for $r = v_*$; and α and β = laminar and turbulent flow resistance coefficients. Kobayashi et al. (2005) modified the formulas of α and β by van Gent (1995) for irregular waves in the form

$$\alpha = \alpha_o \left(\frac{1-n_p}{n_p} \right)^2 \frac{\nu}{D_{n50}^2} \; ; \beta = \left(\beta_1 + \frac{\beta_2}{\sigma_v} \right) ; \beta_1 = \frac{\beta_o \left(1-n_p\right)}{n_p^3 D_{n50}} ; \beta_2 = \frac{7.5 \beta_o \left(1-n_p\right)}{\sqrt{2} n_p^2 T_p} \tag{8}$$

where α_o and β_o = empirical parameters calibrated as α_o = 1,000 and β_o = 5; n_p = porosity of the stone; D_{n50} = nominal stone diameter defined as $D_{n50} = \left(M_{50} / \rho_s\right)^{1/3}$ with M_{50} = median stone mass and ρ_s = stone density; ν = kinematic viscosity of water $\left(\nu \simeq 0.01 \mathrm{cm}^2/\mathrm{s}\right)$; and T_p = spectral peak period. The mean $\bar{v}$ and standard deviation σ_v are estimated assuming the local force balance between the horizontal gradient of hydrostatic pressure and the flow resistance inside the permeable layer

$$\left(\alpha + 1.64 \beta \sigma_v\right) \bar{v} = -g \frac{d\bar{\eta}}{dx} \quad ; \quad \alpha \sigma_v + 1.9 \beta \sigma_v^2 = g k_p \bar{h} \sigma_* \tag{9}$$

where k_p = linear wave number based on $\bar{h}$ and T_p. Eq. (9) can be solved analytically to obtain σ_v and $\bar{v}$ for known $k_p \bar{h} \sigma_*$ and $d\bar{\eta} / dx$.

The energy dissipation rate D_B due to wave breaking in Eq. (1) is estimated using the formula by Battjes and Stive (1985) which is modified by Kobayashi et al. (2005) as

$$D_B = \frac{\rho g a Q H_B^2}{4T_p} \;\; ; \;\; a = \frac{T_p S_b}{b}\left(\frac{g}{\bar{h}}\right)^{0.5} \geq 1 \;\; ;$$
$$\frac{Q-1}{\ln Q} = \left(\frac{H_{\rm rms}}{H_m}\right)^2 \;\; ; \;\; H_m = \frac{0.88}{k_p}\tanh\left(\frac{\gamma k_p \bar{h}}{0.88}\right) \qquad (10)$$

where a = empirical coefficient; Q = fraction of breaking waves with $Q=0$ for no wave breaking and $Q=1$ when all waves break; H_B = wave height used to estimate D_B; S_b = local bottom slope defined as $S_b = dz_b / dx$; b = slope adjustment factor calibrated as $b=3$; $H_{\rm m}$ = local depth-limited wave height with $H_{\rm m} = \gamma \bar{h}$ in shallow water; and γ = breaker ratio parameter. The coefficient a is the ratio between the wavelength and the horizontal length scale $\left(b\bar{h}/S_b\right)$ imposed by the small depth $\bar{h}$ and the bottom slope S_b near the shoreline when $a>1$.

The increase of D_B due to the slope effect results in the increase of q_r in Eq. (3). To offset this increase, use is made of $\beta_r = \left(0.1+S_b\right) \geq 0.1$, which implies that the wave-front slope increases on the upward slope (Kobayashi et al. 2005).

The requirement of $0 \leq Q \leq 1$ implies $H_{\rm rms} \leq H_{\rm m}$ but $H_{\rm rms}$ becomes larger than $H_{\rm m}$ in very shallow water. When $H_{\rm rms} > H_{\rm m}$, use is made of $Q=1$ and $H_B = H_{\rm rms}$ instead of $H_B = H_{\rm m}$ for $H_{\rm rms} \leq H_{\rm m}$. In addition, $\sigma_* = \sigma_\eta / \bar{h}$ in Eqs. (5), (6) and (9) becomes too large due to the local use of linear shallow-water wave theory and use is made of $\sigma_* = \left(\sigma_{*_c} \sigma_\eta / \bar{h}\right)^{0.5}$ if $\sigma_* > \sigma_{*_c} = \gamma / \sqrt{8}$. The values of γ calibrated by Battjes and Stive (1985) were in the range of 0.6 – 0.8. In the subsequent comparisons, γ = 0.6, 0.7 and 0.8 are tried, whereas the other empirical parameters are kept the same as those used by Kobayashi et al. (2005) for the related problem of wave transmission over a submerged porous breakwater.

Eqs. (1) – (10) are solved using a finite difference method with constant nodal spacing Δx of approximately 1 cm for the small-scale experiments in this study. The bottom elevation $z_b(x)$ and the impermeable boundary $z_p(x)$ are specified as input. The stone is characterized by its nominal diameter D_{n50} and porosity n_p. The measured values of $T_p, \overline{\eta}$ and $H_{\rm rms} = \sqrt{8}\,\sigma_\eta$ as well as $q_r = 0$ are specified at the seaward boundary $x = 0$ outside the surf zone. The landward-marching computation is continued until the computed value of $\overline{h}$ or σ_η becomes negative in the region of $\overline{h}$ on the order of 0.1 cm. For the option of IROLL = 0, the roller volume flux $q_r = 0$ and Eq. (3) is not used. The computation time is of the order of one second.

The time-averaged model based on Eqs. (1) – (10) neglects reflected waves. An attempt is made to estimate the degree of wave reflection. The onshore energy flux F in Eq. (1) decreases landward due to wave breaking, bottom friction and porous flow resistance. The residual energy flux F_{sws} at the still water shoreline located at $z_b = 0$ is assumed to be reflected and propagate seaward. This assumption neglects the fact that the landward-marching computation is made without regard to wave reflection. The root-mean-square wave height $(H_{\rm rms})_r$ due to the reflected wave energy flux is crudely estimated as

$$(H_{rms})_r = \left[8F_{sws}/(\rho g C_g)\right]^{0.5} \tag{11}$$

2.2 PROBABILISTIC RUNUP MODEL

A probabilistic model for irregular wave runup is developed using the computed $\overline{\eta}(x)$ and $\sigma_\eta(x)$ on the permeable slope. A runup wire is used in the subsequent experiments to measure the shoreline oscillations above the slope as shown in Fig. 2-1. The vertical height

δ_r of the wire above the average stone surface is known in the following. The wire measures the instantaneous elevation $\eta_r(t)$ above SWL of the intersection between the wire and the free surface unlike a wave gauge that measures $\eta(t)$ at given x. Fig. 2-2 depicts an intuitive method used to estimate the mean $\overline{\eta}_r$ and standard deviation σ_r of $\eta_r(t)$.

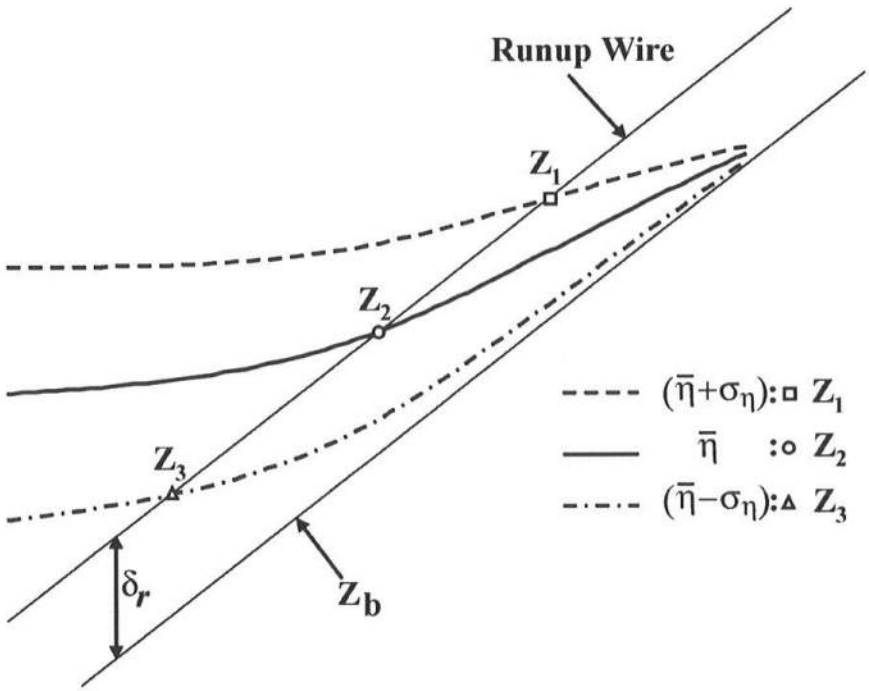

Fig. 2-2: Elevations Z_1, Z_2 and Z_3 of intersections of $\left(\overline{\eta}+\sigma_\eta\right)$, $\overline{\eta}$ and $\left(\overline{\eta}-\sigma_\eta\right)$ with runup wire where $\overline{\eta}$ and σ_η are the mean and standard deviation of free surface elevation.

The probabilities of η exceeding $\left(\overline{\eta}+\sigma_\eta\right)$, $\overline{\eta}$ and $\left(\overline{\eta}-\sigma_\eta\right)$ are assumed to be the same as the probabilities of η_r exceeding $\left(\overline{\eta}_r+\sigma_r\right)$, $\overline{\eta}_r$ and $\left(\overline{\eta}_r-\sigma_r\right)$, respectively. The elevations of Z_1, Z_2 and Z_3 of the intersections of $\left(\overline{\eta}+\sigma_\eta\right)$, $\overline{\eta}$ and $\left(\overline{\eta}-\sigma_\eta\right)$ with the runup wire are obtained using the computed $\overline{\eta}(x)$ and $\sigma_\eta(x)$ together with the wire elevation

$\left[z_b(x)+\delta_r\right]$. The obtained elevations are assumed to correspond to $Z_1=\left(\overline{\eta_r}+\sigma_r\right)$, $Z_2=\overline{\eta_r}$ and $Z_3=\left(\overline{\eta_r}-\sigma_r\right)$. The mean and standard deviation of $\eta_r(t)$ are estimated as

$$\overline{\eta_r}=\left(Z_1+Z_2+Z_3\right)/3 \quad ; \quad \sigma_r=\left(Z_1-Z_3\right)/2 \tag{12}$$

where the use of Z_1, Z_2 and Z_3 to estimate $\overline{\eta}_r$ is slightly more reliable than $\overline{\eta}_r=Z_2$ because the elevation Z_2 is somewhat sensitive to the detailed spatial variation of $\overline{\eta}(x)$.

The runup height R is defined as the crest height above SWL of the temporal variation of η_r. The time series of $\left[\eta_r(t)-\overline{\eta}_r\right]$ is analyzed using a zero-upcrossing method to identify the crests in the time series. This procedure is the same as that used for the analysis of the wave crests in the time series of $\eta(t)$ except that the wave crest is defined as the height above the mean water level. The probability distribution of linear wave crests is normally given by the Rayleigh distribution [e.g., Goda (2000)], whereas Tayfun (2004) presented the distribution of nonlinear wave crests in deep water. As a first approximation, the runup height $\left(R-\overline{\eta}_r\right)$ above the mean level $\overline{\eta}_r$ is given by the Rayleigh distribution

$$P(R)=\exp\left[-2\left(\frac{R-\overline{\eta}_r}{R_{1/3}-\overline{\eta}_r}\right)^2\right] \tag{13}$$

where $P(R)$ = exceedance probability of the runup height R above SWL; and $R_{1/3}$ = significant runup height defined as the average of 1/3 highest values of R. The mean $\overline{\eta}_r$ related to wave setup is normally neglected in Eq. (13) for the prediction of irregular wave runup on steep coastal structures [e.g., van der Meer and Janssen (1995)]. However, wave setup on gentler slopes is not negligible as will be shown for the permeable slope experiments in this study.

Finally, it is necessary to express $R_{1/3}$ in terms of $\overline{\eta_r}$ and σ_r estimated using Eq. (12). If the probability distribution of η_r is approximately Gaussian, use may be made of $\left(R_{1/3}-\overline{\eta_r}\right)\simeq 2\sigma_r$ (Goda 2000). For the following experiments using 1/5 and 1/2 permeable slopes, $R_{1/3}$ is estimated as

$$R_{1/3}=\overline{\eta_r}+\left(2+\tan\theta\right)\sigma_r \tag{14}$$

where θ = slope angle from the horizontal and $\tan\theta$ = 1/5 and 1/2 in the experiments. The slope correction in Eq. (14) is purely empirical and needs to be verified for other slopes.

CHAPTER 3 EXPERIMENTS

Thirty tests under incident irregular waves were conducted to analyze the cross-shore wave evolution and horizontal velocity in the surf zone on a gently sloping impermeable beach and a 1/5 slope with a porous cobble layer. This chapter will review the experimental setup for the 1/5 slope experiment and summarize the experiment conducted by Kearney and Kobayashi (2000) with a 1/2 slope stone revetment. The measurement procedures of the free surface elevation, runup and velocities are explained in the subsequent sections. The obtained data were used to validate the numerical wave model and the probabilistic runup model.

3.1 EXPERIMENTAL SETUP FOR 1/5 SLOPE TESTS

The experiment was conducted in a wave flume in the Ocean Engineering Laboratory of the University of Delaware, that was 33 m long, 0.6 m wide and 1.5 m high as shown in Fig. 3-1. An impermeable smooth beach with a 1/34.4 slope was installed in the flume. Angular stone was placed on a 1/5 impermeable slope to simulate an idealized cobble beach. The nominal diameter and porosity of the stone were D_{n50} = 3.4 cm and n_p = 0.5,

respectively. The vertical thickness of the stone layer was 14 cm. No stone movement was detected during the experiment.

Irregular waves, based on the TMA spectrum, were generated in a burst of 429.6 s using a piston-type wave paddle. The sampling rate was 20 Hz for all the time series measured in the experiment. The initial transient of 20 s in each burst was removed for subsequent data analyses.

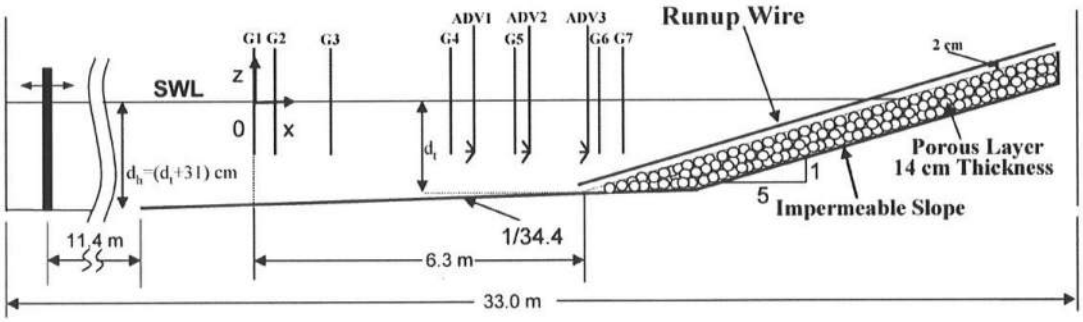

Instrument	G1	G2	G3	G4	G5	G6	G7	ADV1	ADV2	ADV3
Location x=[m]	0	0.308	1.308	4.008	5.618	6.588	6.878	4.268	5.908	6.478

Fig. 3-1: Experimental setup for 1/5 slope tests.

Thirty tests were conducted for the 1/5 slope experiment. The still water depth d_t at the toe of the slope was varied from 16.6 cm to 24.6 cm with an increment of 2 cm. The spectral peak period T_p was approximately 1.5, 2.3 and 3.0 s. Table 1 lists the measured values of T_p and H_{rms} at wave gauge 1 located in the still water depth d_1, as well as the incident root-mean-square wave height $(H_{rms})_i$, and the average reflection coefficient r defined as $r = (H_{\rm rms})_r / (H_{\rm rms})_i$ where $(H_{\rm rms})_r$ and $(H_{\rm rms})_i$ are the reflected and incident root-mean-square wave heights obtained using wave gauges 1 – 3 (Kobayashi et al., 1990). $H_{\rm rms}$ includes both incident and reflected waves. The difference between $H_{\rm rms}$ and $(H_{\rm rms})_i$ was less than 5% because $r = 0.16 - 0.24$ and wave gauge 1 was located at the horizontal distance

of 6.3 m seaward of the toe of the 1/5 slope. The root-mean-square wave height $H_{\rm rms} = \sqrt{8}\,\sigma_\eta$ was selected to be as large as feasible without any wave breaking in the vicinity of the wavemaker located in the still water depth $d_h = (d_t + 31)$ cm. For the specified d_t and T_p, two tests were performed to check the variability of $H_{\rm rms}$ resulting from the generation of large waves. Table 1 lists only one of the two repeated tests for brevity but both tests are included in the following data analysis.

Table 1: Wave characteristics at wave gauge 1 for the 1/5 slope experiment.

Test	d_t [cm]	d_1 [cm]	T_p [s]	H_{rms} [cm]	$(H_{rms})_i$ [cm]	r
R16A1	16.6	34.9	1.53	10.04	9.62	0.17
R16B1	16.6	34.9	2.31	10.47	10.07	0.20
R16C1	16.6	34.9	3.10	6.76	6.66	0.24
R18A1	18.6	36.9	1.53	10.54	10.18	0.17
R18B1	18.6	36.9	2.31	9.66	9.25	0.18
R18C1	18.6	36.9	3.09	7.19	6.98	0.23
R20A1	20.6	38.9	1.53	10.94	10.71	0.16
R20B1	20.6	38.9	2.31	11.49	11.05	0.19
R20C1	20.6	38.9	2.96	7.43	7.21	0.22
R22A1	22.6	40.9	1.53	11.43	11.16	0.17
R22B1	22.6	40.9	2.31	12.08	11.53	0.19
R22C1	22.6	40.9	2.90	7.81	7.47	0.23
R24A1	24.6	42.9	1.59	11.59	11.29	0.17
R24B1	24.6	42.9	2.31	12.22	11.72	0.20
R24C1	24.6	42.9	2.90	7.96	7.59	0.23

d_t = toe depth; d_1 =still water depth at wave gauge 1; T_p = spectral peak period; H_{rms} = root-mean-square wave height; $(H_{rms})_i$ = incident H_{rms}; r = average reflection coefficient.

3.2 EXPERIMENTAL SETUP FOR 1/2 SLOPE TESTS

The 1/2 slope tests were reported concisely by Kearney and Kobayashi (2000) but they are summarized here for the sake of completeness. The experiment was conducted in a wave tank that was 30 m long, 2.44 m wide, and 1.5 m high. A plywood beach with a 1/32.1 slope and a stone revetment with a 1/2 slope were installed in the tank. The nominal diameter of the stone was D_{n50} = 3.2 cm and the stone porosity, which was not measured, is assumed to be the same as n_p = 0.5 for the stone used in the 1/5 slope experiment. The thickness of the

permeable layer was approximately 14 cm. A runup wire was placed at a distance of δ_r = 2.5 cm above the 1/2 stone revetment. Ten wave gauges were arranged like in Fig. 2-1 to measure the irregular wave transformation from outside the surf zone to the toe of the 1/2 slope. Wave gauge 1 was located 14.8 m seaward of the toe. One ADV was also placed at the toe. Twenty-seven tests were conducted for the spectral peak periods T_p = 1.5, 2.4 and 4.7 s of the TMA spectra and nine different toe depths d_t = 4 – 20 cm with an increment of 2 cm. The repeatability of each test was checked but the repeated test results were not reported. The duration of each test and the sampling rate were 400 s and 20 Hz for T_p = 1.5 and 2.4 s and 800 s and 10 Hz for T_p = 4.7 s. The initial transition of 1,200 data points was removed before the data analyses. The wave characteristics and the reflection coefficient r at wave gauge 1 for the 27 tests are listed in Table 2. The values of r were slightly larger for the 1/2 slope than for the 1/5 slope.

Table 2: Wave characteristics at wave gauge 1 for the 1/2 slope experiment.

Test	d_t [cm]	d_1 [cm]	T_p [s]	H_{rms} [cm]	$(H_{rms})_i$ [cm]	r
A20	20.0	66.1	4.7	16.4	15.8	0.33
A18	18.0	64.1	4.7	16.0	15.1	0.32
A16	16.0	62.1	4.7	14.7	15.3	0.34
A14	14.0	60.1	4.7	14.3	14.5	0.28
A12	12.0	58.1	4.7	13.9	14.4	0.27
A10	10.0	56.1	4.7	13.7	14.0	0.28
A8	8.0	54.1	4.7	13.7	13.2	0.27
A6	6.0	52.1	4.7	12.4	12.9	0.26
A4	4.0	50.1	4.7	12.7	12.5	0.26
B20	20.0	66.1	2.4	11.4	13.8	0.36
B18	18.0	64.1	2.4	10.9	13.4	0.36
B16	16.0	62.1	2.4	10.3	13.2	0.36
B14	14.0	60.1	2.4	9.9	12.9	0.35
B12	12.0	58.1	2.4	9.9	12.6	0.34
B10	10.0	56.1	2.4	10.0	12.3	0.30
B8	8.0	54.1	2.4	9.1	11.9	0.32
B6	6.0	52.1	2.4	9.2	11.6	0.29
B4	4.0	50.1	2.4	9.1	11.3	0.26
C20	20.0	66.1	1.5	9.7	10.0	0.23
C18	18.0	64.1	1.5	9.4	9.7	0.22
C16	16.0	62.1	1.5	9.4	9.4	0.23
C14	14.0	60.1	1.5	9.1	9.2	0.24
C12	12.0	58.1	1.5	8.9	9.0	0.24
C10	10.0	56.1	1.5	8.8	8.9	0.22
C8	8.0	54.1	1.5	8.6	8.8	0.20
C6	6.0	52.1	1.5	8.4	8.6	0.20
C4	4.0	50.1	1.5	8.4	8.5	0.20

d_t = toe depth; d_1 =still water depth at wave gauge 1; T_p = spectral peak period; H_{rms} = root-mean-square wave height; $(H_{rms})_i$ = incident H_{rms}; r = average reflection coefficient.

3.3 FREE SURFACE AND RUNUP MEASUREMENTS

For each test, seven capacitance-type wave gauges and a runup wire were used to measure the time series of η and η_r for the 1/5 slope experiment at the locations indicated in Fig. 3-1 where $x = 0$ at wave gauge 1. Wave gauges 1 – 3 were located immediately outside the surf zone and used to separate the incident and reflected waves using linear wave theory (Kobayashi et al. 1990). Wave gauges 4 – 7 measured the irregular breaking wave transformation on the gentle slope and the seaward edge of the 1/5 porous slope. Calibration of all the wave gauges was performed frequently to ensure the reliability of the measurements.

A capacitance-type runup wire was placed parallel to the 1:5 porous slope to measure the shoreline oscillations above the slope as shown in Fig. 3-1. The vertical height δ_r of the runup wire above the slope was approximately 2 cm. The wire measures the instantaneous elevation $\eta_r(t)$ above SWL of the intersection between the wire and the free surface. The runup wire was calibrated simultaneously as the wave gauges. Because the runup wire was much longer than the wire used for the wave gauges, an extra capacitor was added in series in such a way that the entire length of the wire could be used for the runup measurement. Due to this modification, a third order fit was used for the runup wire calibration.

Table 3 shows the mean and standard deviation of η at wave gauge 6, located at the toe of the porous slope, and the shoreline elevation η_r above SWL measured by the runup wire as well as $R_{1/3}$= significant runup height above SWL and $R_{2\%}$= runup height corresponding to 2% exceedance probability. Wave setup $\bar{\eta}$ at the toe of the 1:5 porous slope is in the range of 0-0.3 cm, while $\bar{\eta}_r$ is in the range of 1-3 cm. The standard deviations σ_η and σ_r are on the same order of magnitude for the 1:5 porous slope.

Table 3: Mean and standard deviation of free surface elevation at wave gauge 6 and corresponding runup statistics for the 1/5 slope experiment.

Test	Wave Gauge 6		Wave Runup Wire			
	$\bar{\eta}$ [cm]	σ_η [cm]	$\bar{\eta}_r$ [cm]	σ_r [cm]	$R_{1/3}$ [cm]	$R_{2\%}$ [cm]
R16A1	0.28	2.88	1.27	2.28	5.82	7.41
R16B1	0.29	2.92	1.55	3.09	8.19	11.29
R16C1	0.04	2.40	0.77	2.90	7.69	10.73
R18A1	0.26	3.14	1.94	2.51	7.42	9.70
R18B1	0.16	2.94	2.02	3.29	9.57	11.61
R18C1	0.05	2.41	1.34	3.33	9.86	12.43
R20A1	0.23	3.38	2.47	2.90	8.98	10.62
R20B1	0.19	3.34	2.38	3.90	11.03	13.61
R20C1	-0.01	2.48	1.99	3.66	11.01	14.12
R22A1	0.25	3.49	2.70	2.95	9.06	11.10
R22B1	0.17	3.53	3.18	4.31	12.19	14.31
R22C1	0.04	2.49	1.82	4.19	11.58	15.20
R24A1	0.21	3.66	2.73	2.92	8.67	10.54
R24B1	0.06	3.82	2.56	4.23	10.69	12.33
R24C1	0.01	2.56	1.67	4.09	10.38	13.09

3.4 VELOCITY MEASUREMENTS

Three 3D acoustic Doppler velocimeters (ADV) were used to measure fluid velocities at the approximate middle between the still water level and the beach. ADV3 located at the toe of the 1:5 slope was lowered for the tests with d_t= 16.6 and 18.6 cm to avoid exposure to air during wave rundown. The cross-shore locations of the three ADVs are given in Fig. 3-1. The measured vertical and cross-flume velocities appeared to be dominated by turbulent velocities and were much smaller than the cross-shore velocity u which was dominated by the wave component. Only the horizontal velocity u is considered hereafter.

CHAPTER 4 PROBABILITY DISTRIBUTIONS

The statistics of the measured time series of the free surface and shoreline elevations as well as the cross-shore horizontal velocity are examined in this chapter. The measured probability density functions of these variables are compared with the exponential gamma distribution and the Gaussian distribution in the same way as in Kobayashi et al. (1998). A brief description of the exponential gamma distribution is given first. The distributions for the measured wave heights and runup heights are also compared with the Rayleigh and Weibull distributions, where the setup effect on the runup height is examined.

4.1 EXPONENTIAL GAMMA DISTRIBUTION

The measured normalized free surface elevation $\eta_* = \left(\eta - \overline{\eta}\right)/\sigma_\eta$ and the normalized cross-shore horizontal velocity $u_* = \left(u - \overline{u}\right)/\sigma_u$ are compared with the exponential gamma

distribution described in the report by Orzech and Kobayashi (1997). The exponential gamma distribution for η_* is expressed as

$$f(\eta_*) = \left[\Gamma(a)\right]^{-1} \sqrt{\psi'(a)} \exp(-ay) \exp\left[-\exp(-y)\right] \tag{15}$$

$$y = \sqrt{\psi'(a)}\eta_* - \psi(a) \tag{16}$$

where a = shape parameter, Γ = gamma function, ψ = digamma function and ψ' = trigamma function. The relationship between the skewness, s, and the shape parameter a is given by

$$s = -\psi''(a)\left[\psi'(a)\right]^{-\frac{3}{2}} \tag{17}$$

where ψ'' = tetragamma function. The kurtosis of, K, is given by

$$K = \psi'''(a)\left[\psi'(a)\right]^{-2} + 3 \tag{18}$$

where ψ''' = pentagamma function. The gamma and related functions are explained by Abramowitz and Stegun (1972) and tabulated by Gran (1992).

The Gaussian and the exponential distributions are special cases of the exponential gamma distribution when the skewness s equals 0 and 2, respectively:

$$\textit{Gaussian}: \quad f(\eta_*) = \frac{1}{\sqrt{2\pi}} \exp\left(-\eta_*^2/2\right) \quad \textit{for} \quad s = 0 \tag{19}$$

$$\textit{Exponential}: \quad f(\eta_*) = \exp\left[-(\eta_* + 1)\right] \quad \textit{for} \quad s = 2 \tag{20}$$

4.2 FREE SURFACE AND SHORELINE ELEVATIONS

The statistics of the measured time series of the free surface and shoreline elevations η and η_r are examined first. The normalized free surface elevation η_* is defined as

$$\eta_* = \frac{\eta - \bar{\eta}}{\sigma_\eta} \tag{21}$$

where $\bar{\eta}$ and σ_η are the mean and standard deviation of η. For the runup elevation η_r, $\bar{\eta}$ and σ_η are replaced by $\bar{\eta}_r$ and σ_r. The mean and standard deviation of η_* are zero and unity. Kobayashi et al. (1998) compared the measured probability density functions for η_* and u_* with the Gaussian and exponential gamma distributions using the measured values of mean, standard deviation and skewness.

Fig. 4-1 and Fig. 4-2 show the measured probability density functions at wave gauges 1 - 7 and the runup wire for the 30 tests in the 1/5 slope experiment. Wave gauges 1, 2 and 3 are located just seaward of the surf zone, wave gauge 4 and 5 approximately in the middle of the surf zone, wave gauge 6 at the toe of the porous slope and wave gauge 7 on the permeable slope. The shoreline elevation above SWL measured by the runup wire is analyzed in the same way as the free surface elevations. The theoretical exponential gamma distribution is also plotted in Fig. 4-1 and Fig. 4-2 using the average value of the measured skewness, s, for all the tests at each wave gauge location. It should be noted that the agreement with the data for each specific test is better when the measured skewness for the specific test is utilized instead of the average value of the skewness for all the tests at the same wave gauge location. The Gaussian distribution is also plotted in Fig. 4-1 and Fig. 4-2 for comparison. Fig. 4-1 and Fig. 4-2 show the skewed wave profiles in the surf zone with peaked crests and flat troughs caused by wave nonlinearities. The agreement for the exponential gamma distribution is good. Nevertheless, the adoption of the exponential gamma distribution for prediction purposes is not convenient because the skewness is hard to estimate accurately. The Gaussian distribution is a good first approximation for the free surface elevation well outside the surf

zone and the shoreline elevation. The Gaussian distribution of the shoreline elevation is made implicitly in Eqs. (13) and (14).

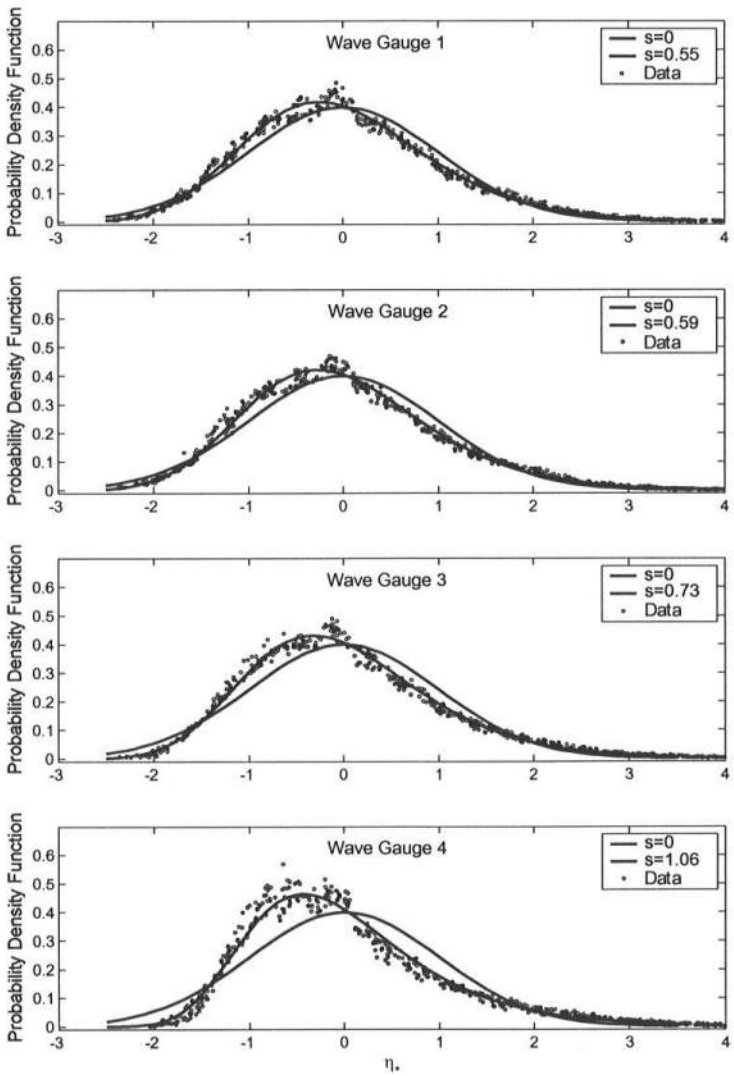

Fig. 4-1: Measured and computed probability density functions of normalized free surface elevation η_* at wave gauges 1 - 4 for all the 1/5 slope tests.

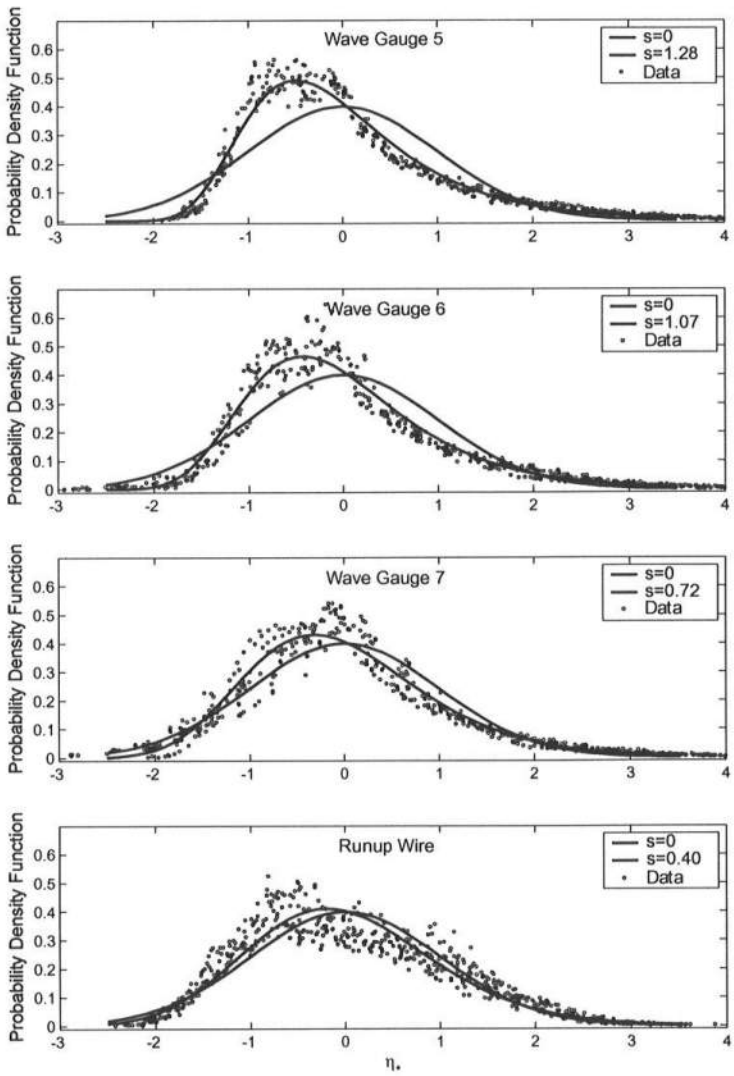

Fig. 4-2: Measured and computed probability density functions of normalized free surface elevation η_* at wave gauges 5 - 7 and by runup wire for all the 1/5 slope tests.

4.3 CROSS-SHORE VELOCITY

The statistics of the measured time series of the cross-shore horizontal velocity u is examined in the same manner as the free surface elevation. The normalized cross-shore horizontal velocity u_* is defined as

$$u_* = \frac{u - \bar{u}}{\sigma_u} \tag{22}$$

where $\bar{u}$ and σ_u are the measured mean and standard deviation of u.

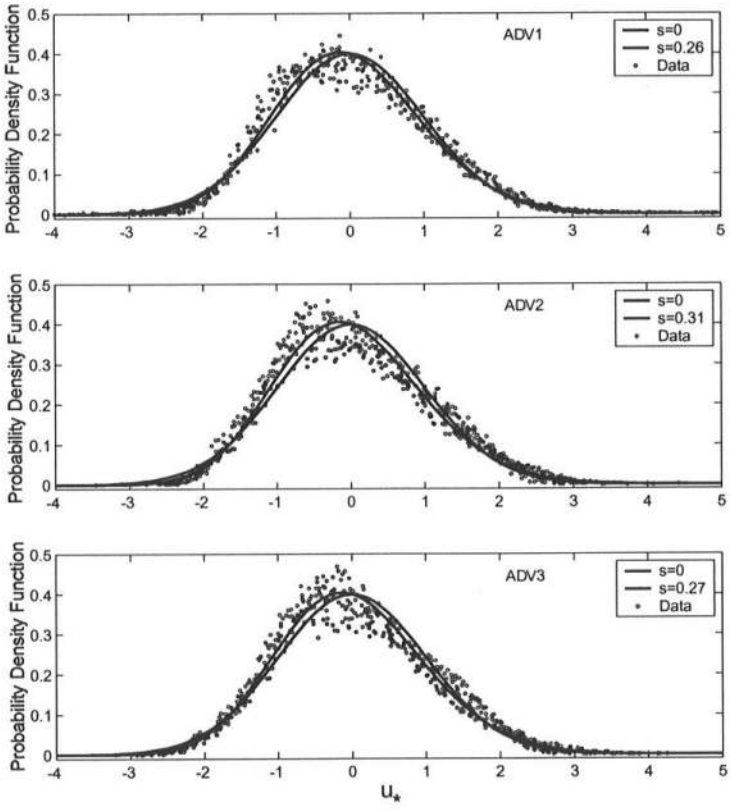

Fig. 4-3: Measured and computed probability density functions of normalized cross-shore horizontal velocity u_* at ADV1, ADV2 and ADV3 for all the 1/5 slope tests.

Fig. 4-3 shows the comparison between the measured probability density function of the normalized cross-shore horizontal velocity u_* and the exponential gamma distribution using the average value of the measured skewness, s_u, for all the tests at each velocimeter location. The measured skewness, s_u, is in the range of 0 - 0.50 and the Gaussian distribution is a good approximation. It is noted that the skewness is smaller for the horizontal velocity than for the free surface, implying that the nonlinearity decreases downward from the free surface. The Gaussian distribution of the horizontal velocity u is assumed to derive Eq. (4).

4.4 WAVE HEIGHT DISTRIBUTION

The measured exceedance probability distributions of the zero-upcrossing wave height H at each wave gauge location is compared with the Rayleigh and Weibull distributions given by

$$Rayleigh: \quad P = \exp\left[-2\left(H / H_{1/3}\right)^2\right] \tag{23}$$

$$Weibull: \quad P = \exp\left[-\beta\left(H / H_{1/3}\right)^{\alpha}\right] \tag{24}$$

with P = exceedance probability, $H_{1/3}$ = measured significant wave height for each time series, α = shape parameter and β is a nondimensional parameter related to the scale parameter of the Weibull distribution. Eq. (24) reduces to Eq. (23) when $\alpha = 2$ and $\beta = 2$.

Fig. 4-4 and Fig. 4-5 compare the measured exceedance probability distributions of the wave heights H at wave gauges 1 - 7 with the Rayleigh distribution given by Eq. (23). These figures include all the data points from the 30 tests in the 1/5 slope experiment.

Fig. 4-6 and Fig. 4-7 compare the measured exceedance probability distributions of H with the Weibull distribution given by Eq. (24) at wave gauges 1-7 for the test R20B1, as

an example. The Rayleigh distribution is also plotted for reference. The parameters α and β are estimated for each measured distribution using the maximum likelihood method. Table 4 shows the estimates of the Weibull parameters α and β for the different 1/5 slope tests at each wave gauge location. Due to the fact that α and β are fitted for each distribution, the agreement with the measured distribution is slightly better for the Weibull distribution. However, for prediction purposes, it is difficult to use the Weibull distribution because α and β are hard to estimate in advance.

As a whole, the Rayleigh distribution is a good approximation except that the scatter of data points is large for very small P partly because the test duration of 429.6 s was not very long.

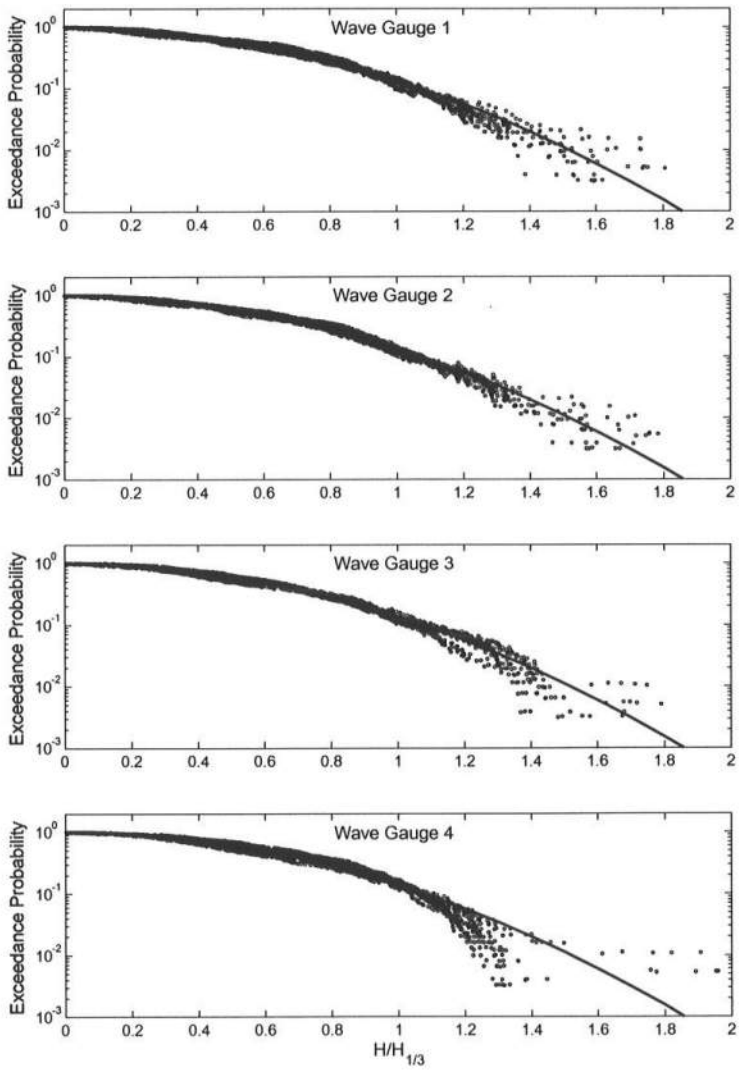

Fig. 4-4: Measured and Rayleigh exceedance probability distributions of wave heights at wave gauges 1 - 4 for all the 1/5 slope tests.

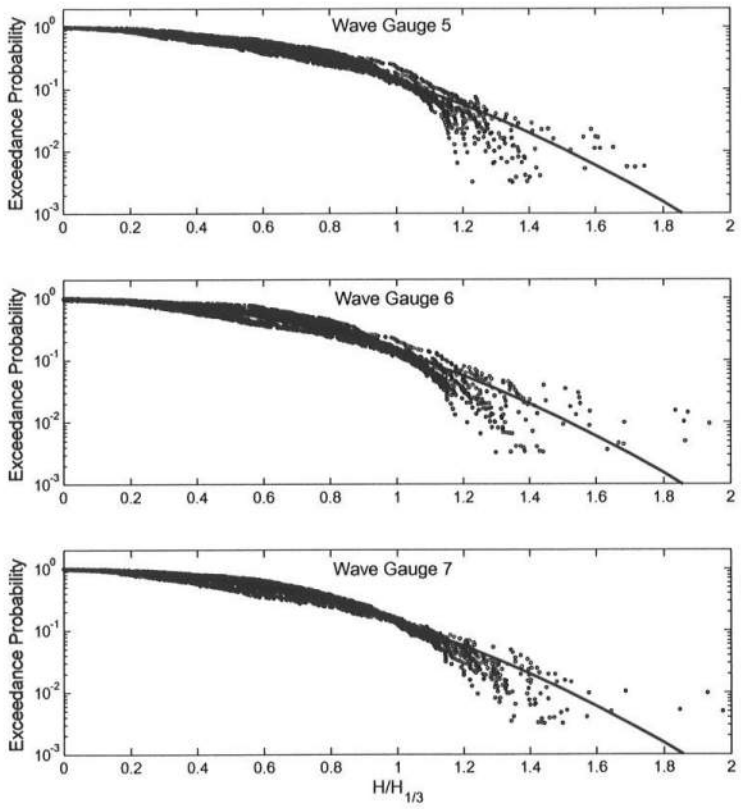

Fig. 4-5: Measured and Rayleigh exceedance probability distributions of wave heights at wave gauges 5 - 7 for all the 1/5 slope tests.

Table 4: Estimates of Weibull parameters at each wave gauge for all the 1/5 slope tests.

TEST	Gauge 1		Gauge 2		Gauge 3		Gauge 4		Gauge 5		Gauge 6		Gauge 7	
	α	β	α	β	α	β	α	β	α	β	α	β	α	β
R16A1	2.10	2.06	2.09	2.05	2.11	2.02	2.47	2.02	2.33	1.93	2.88	1.90	2.23	1.88
R16B1	2.12	2.05	2.11	2.03	2.10	2.08	2.29	2.04	2.21	2.01	2.28	2.01	2.28	2.02
R16C1	1.68	2.04	1.64	2.02	1.70	2.04	1.70	2.06	1.48	2.08	1.60	2.11	1.75	2.05
R18A1	2.14	2.06	1.95	1.91	2.05	2.00	2.43	2.00	2.36	1.95	2.46	1.91	2.20	2.16
R18B1	2.20	2.02	2.15	2.03	1.95	2.07	1.99	2.06	1.98	2.10	2.15	2.08	1.89	2.05
R18C1	1.55	2.06	1.63	2.05	1.67	2.08	1.76	2.09	1.57	2.09	1.54	2.10	1.52	2.10
R20A1	2.04	2.05	2.12	2.14	2.18	2.01	2.19	2.00	2.24	1.96	2.37	1.97	2.28	1.97
R20B1	2.11	2.01	2.04	2.03	2.05	2.07	2.13	2.07	2.16	2.07	2.30	2.04	1.95	2.04
R20C1	1.58	2.06	1.72	2.04	1.90	2.09	1.87	2.08	1.56	2.09	0.94	1.80	1.48	1.96
R22A1	2.09	2.09	2.05	2.07	2.10	2.04	2.21	2.03	2.22	2.01	2.22	1.98	2.03	1.97
R22B1	2.11	2.03	2.05	2.04	2.00	2.08	2.10	2.06	1.98	2.02	2.27	0.83	2.32	1.61
R22C1	1.67	2.04	1.72	2.01	1.84	2.07	1.88	2.06	1.66	2.10	1.71	2.09	1.50	2.06
R24A1	2.03	2.02	2.04	2.07	2.08	2.04	2.27	2.06	1.89	1.98	2.20	1.97	2.23	1.97
R24B1	2.23	2.02	2.03	2.05	2.02	2.11	2.22	2.09	2.00	2.05	1.90	2.02	2.02	2.08
R24C1	1.67	1.99	2.06	2.04	2.03	2.05	2.03	2.06	1.75	2.06	1.90	1.79	1.55	2.03

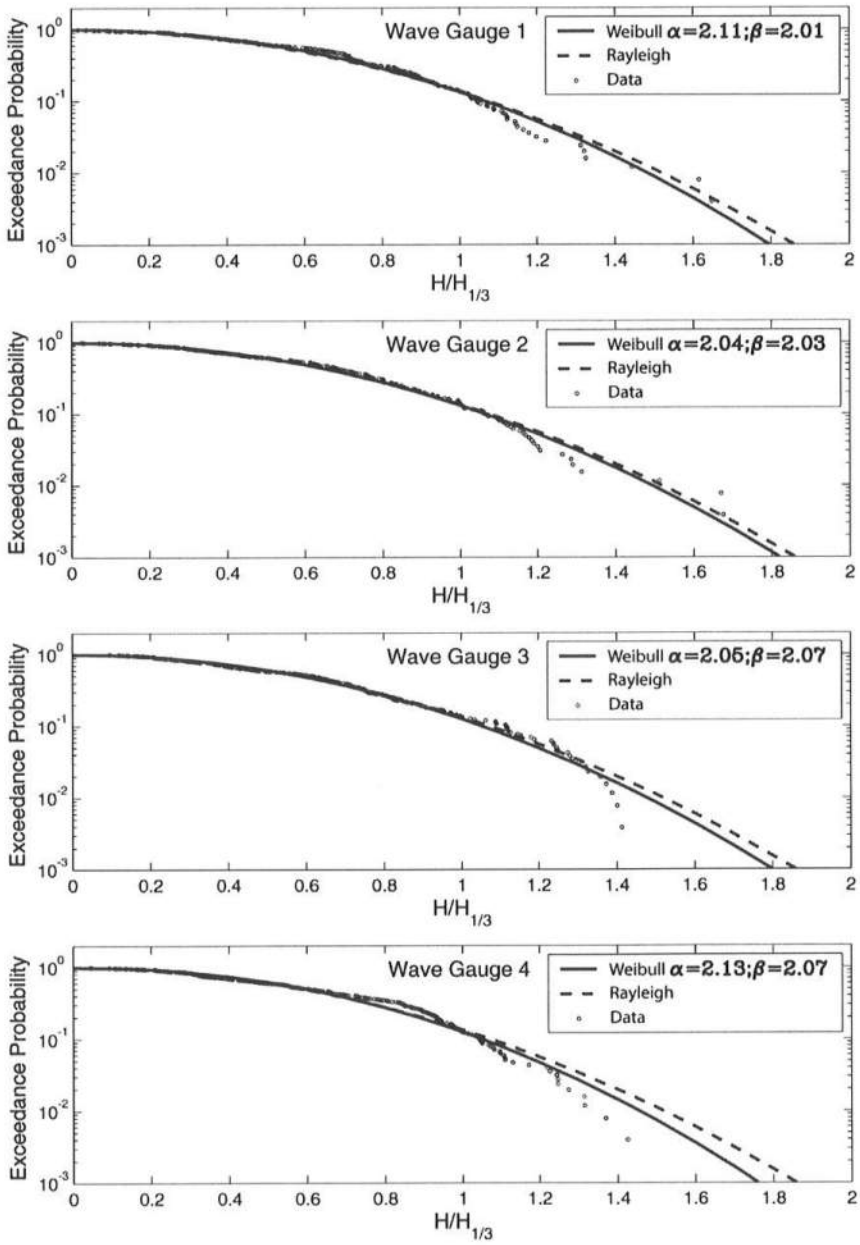

Fig. 4-6: Measured, Rayleigh and Weibull exceedance probability distributions of wave heights at wave gauges 1 - 4 for test R20B1 on 1/5 slope.

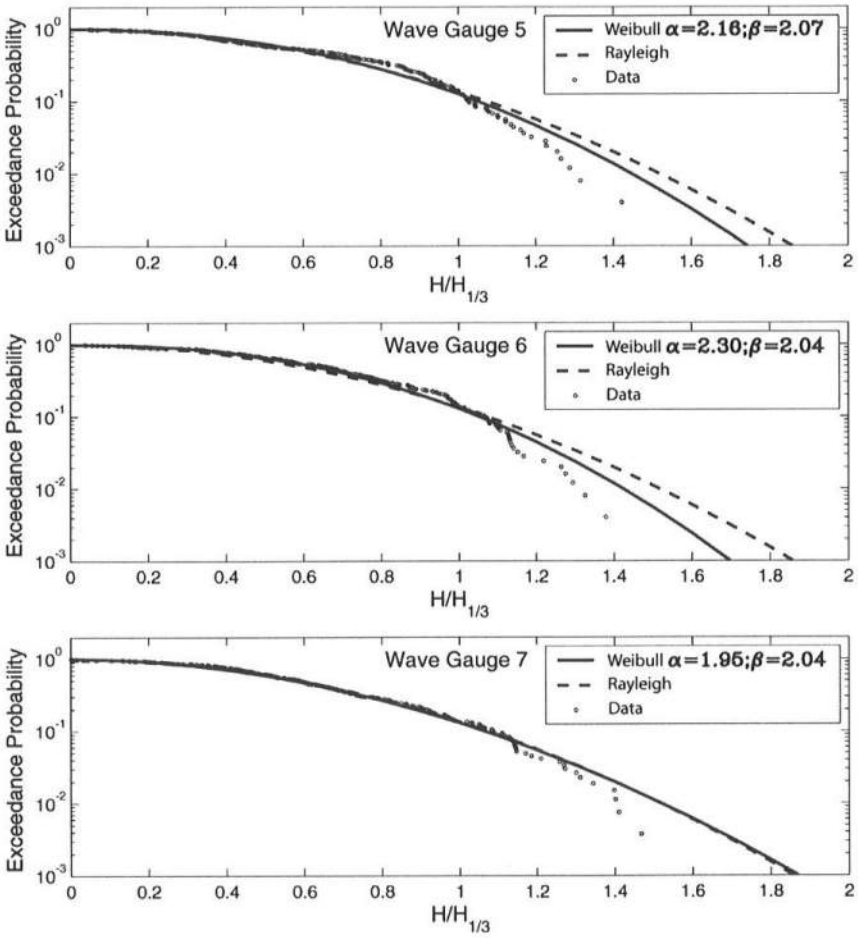

Fig. 4-7: Measured, Rayleigh and Weibull exceedance probability distributions of wave heights at wave gauges 5 - 7 for test R20B1 on 1/5 slope.

4.5 WAVE RUNUP DISTRIBUTION

Fig. 4-8 and Fig. 4-9 compare the measured probability distributions of zero-upcrossing runup heights with the Rayleigh distribution given by Eq. (13) which accounts for the mean $\overline{\eta}_r$ for the runup height R above SWL, and the standard Rayleigh distribution $P(R) = \exp\left[-2\left(R/R_{1/3}\right)^2\right]$, with no regard to the wave setup. Fig. 4-8 includes all the data

points from the 30 tests in the 1/5 slope experiment, while Fig. 4-9 all the data for the 27 tests in the 1/2 slope experiment. The Rayleigh distribution is a good approximation except for the scatter of data points for the exceedance probabilities of the order of 0.01 or less. The agreement for the standard Rayleigh distribution without the wave setup is worse for the 1/5 slope but is similar for the 1/2 slope because the wave setup is appreciable on the 1/5 slope and should be accounted for.

In the same manner as in Figs. 4-6 and 4-7 for the wave height distributions, Fig. 4-10 compares the measured exceedance probability distributions of runup heights as a function of $\left(R-\overline{\eta_r}\right)/\left(R_{1/3}-\overline{\eta_r}\right)$ and $R/R_{1/3}$ for test R20B1 with Weibull and Rayleigh distributions. Table 5 lists the Weibull parameters α and β estimated using the maximum likelihood method. The values of α and β are not too different from two when the wave setup is accounted for.

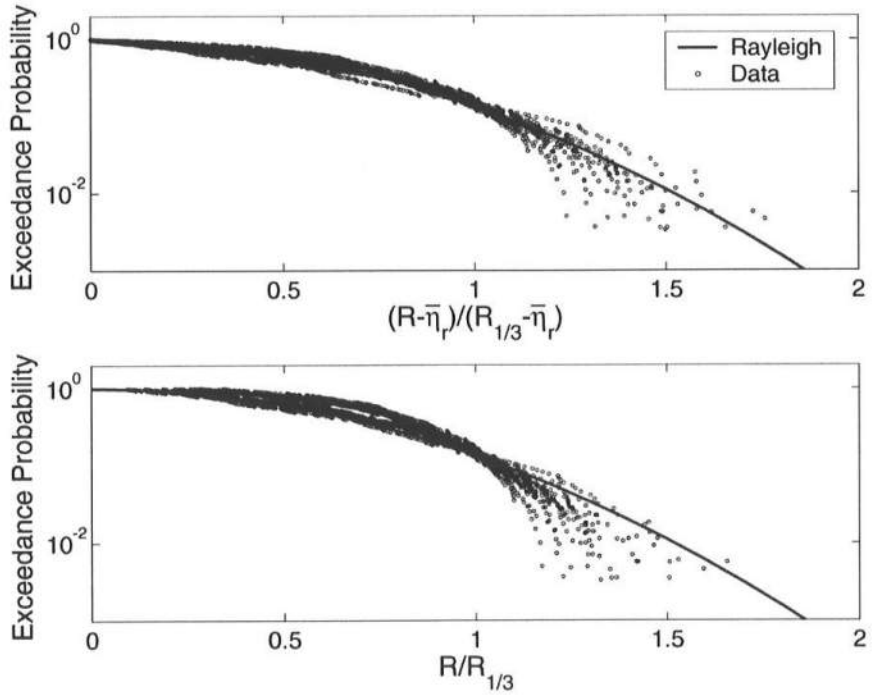

Fig. 4-8: Measured and Rayleigh exceedance probability distributions of runup heights as a function of $\left(R-\overline{\eta_r}\right)/\left(R_{1/3}-\overline{\eta_r}\right)$ and $R/R_{1/3}$ for all the 1/5 slope tests.

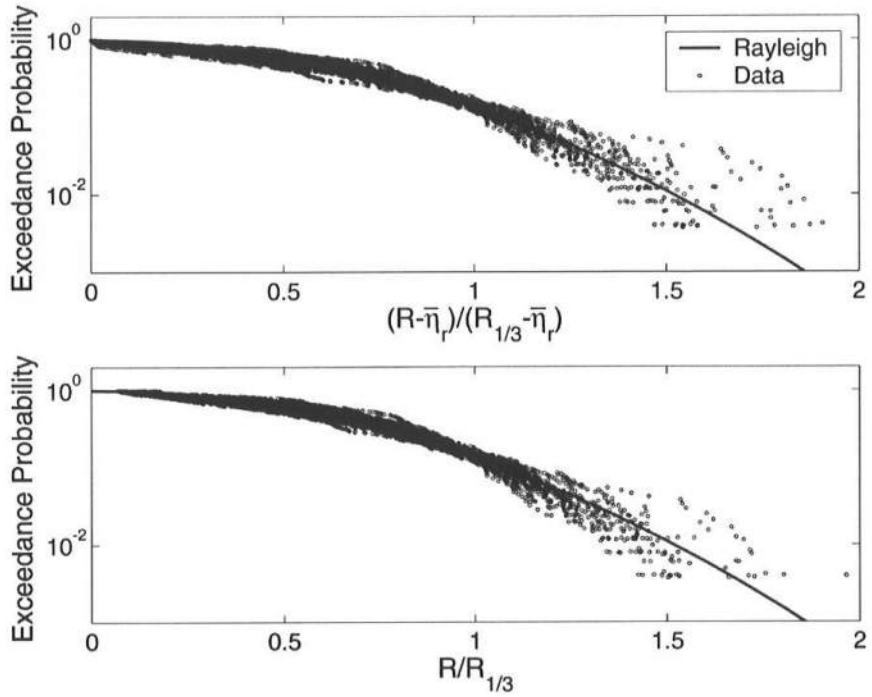

Fig. 4-9: Measured and Rayleigh exceedance probability distributions of runup heights as a function of $\left(R-\overline{\eta_r}\right)/\left(R_{1/3}-\overline{\eta_r}\right)$ and $R/R_{1/3}$ for all the 1/2 slope tests.

Table 5: Estimates of Weibull parameters for runup heights in the 1/5 slope experiment.

TEST	$\left(R-\overline{\eta_r}\right)/\left(R_{1/3}-\overline{\eta_r}\right)$		$R/R_{1/3}$	
	α	β	α	β
R16A1	2.13	1.89	3.29	1.90
R16B1	1.68	1.97	2.57	1.98
R16C1	1.42	1.91	1.98	1.99
R18A1	1.64	2.03	2.92	2.06
R18B1	1.48	1.96	2.59	2.05
R18C1	1.41	2.07	2.06	2.14
R20A1	1.89	1.96	3.48	2.04
R20B1	1.75	1.88	3.03	1.97
R20C1	1.14	1.95	2.10	2.09
R22A1	1.92	1.93	3.70	2.00
R22B1	1.65	1.88	3.28	2.01
R22C1	1.38	1.91	2.26	2.02
R24A1	1.50	1.86	3.37	1.97
R24B1	2.00	1.90	3.53	2.00
R24C1	1.51	1.95	2.36	2.03

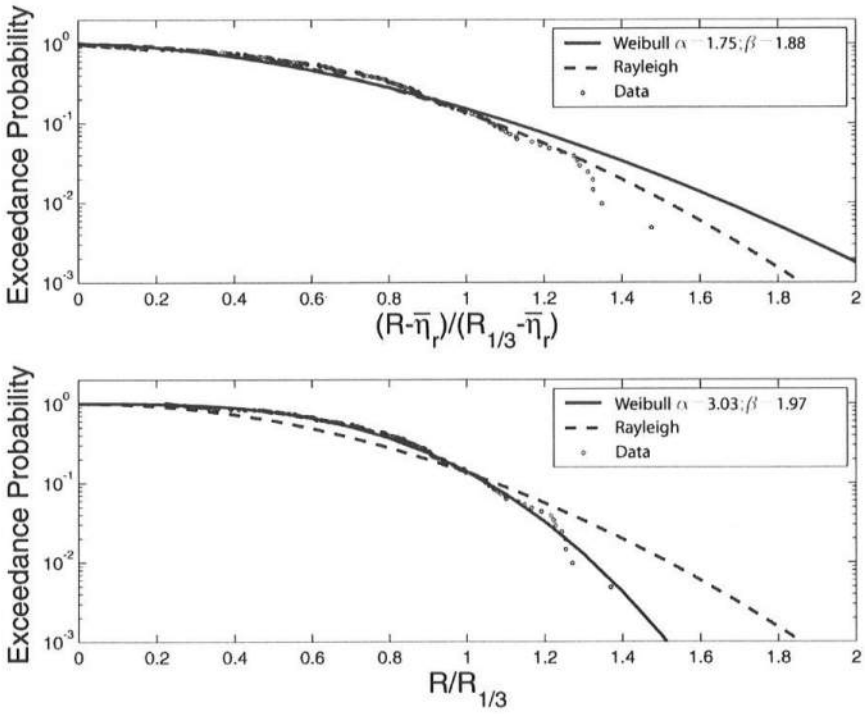

Fig. 4-10: Measured, Rayleigh and Weibull exceedance probability distributions of runup heights as a function of $\left(R-\overline{\eta_r}\right)/\left(R_{1/3}-\overline{\eta_r}\right)$ and $R/R_{1/3}$ for test R20B1 on 1/5 slope.

Fig. 4-11 shows the relationship between the 2% runup height $R_{2\%}$ and significant runup height $R_{1/3}$ for each of the 57 tests where Eq. (13) yields

$$R_{2\%}-\overline{\eta_r}=1.4\left(R_{1/3}-\overline{\eta_r}\right) \tag{25}$$

It is noted that $R_{2\%}$ is used for the design of the crest height of a dike in The Netherlands (van Gent 2001). Fig. 4-11 indicates that Eq. (25) based on the Rayleigh distribution with the wave setup effect slightly overpredicts $R_{2\%}$ for given $R_{1/3}$ and $\overline{\eta}_r$. The degree of the overprediction increases when the measured values of $R_{2\%}$ and $R_{1/3}$ are compared with $R_{2\%}=1.4R_{1/3}$ without the wave setup effect, as can be seen in Fig. 4-12.

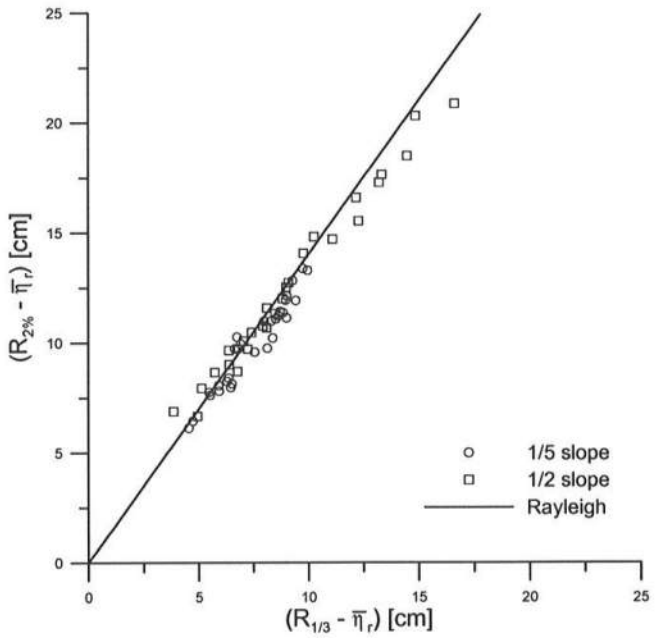

Fig. 4-11: Relationship between $\left(R_{2\%} - \overline{\eta_r}\right)$ and $\left(R_{1/3} - \overline{\eta_r}\right)$ for 1/5 and 1/2 slope tests.

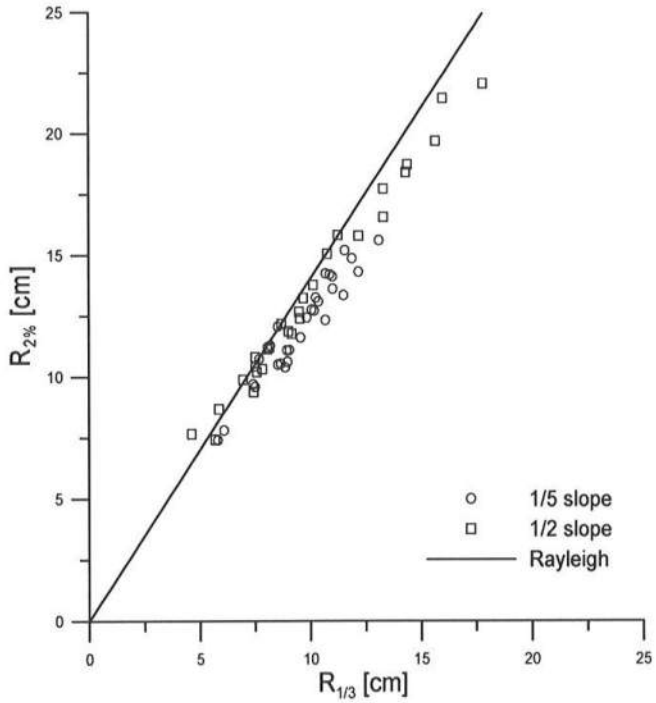

Fig. 4-12: Relationship between $R_{2\%}$ and $R_{1/3}$ for 1/5 and 1/2 slope tests.

Fig. 4-13 examines the accuracy of Eq. (14) for $\tan\theta = 1/5$ and 1/2. The slope correction term ($\sigma_r \tan\theta$) improves the agreement in comparison with $\left(R_{1/3} - \overline{\eta}_r\right) = 2\sigma_r$ based on the Gaussian shoreline fluctuations. This slope correction will not be valid when the slope becomes steeper and the slope angle θ approaches 90°.

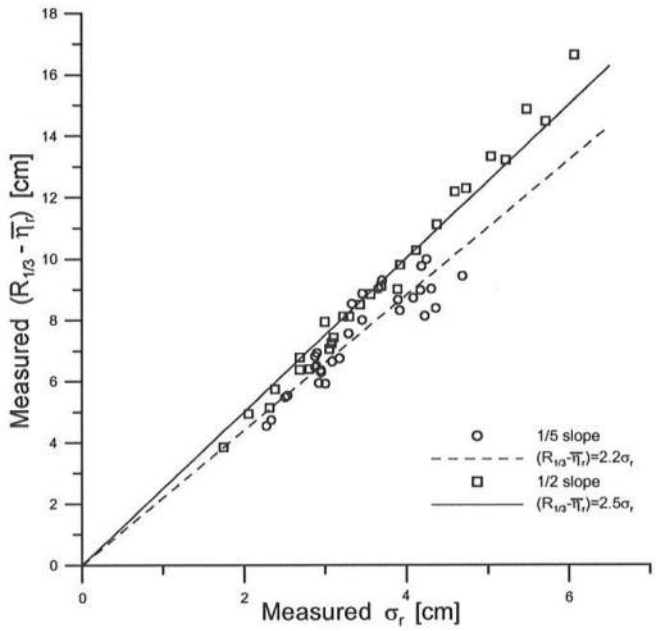

Fig. 4-13: Empirical formula $\left(R_{1/3} - \overline{\eta_r}\right) = 2.2\sigma_r$ and $2.5\sigma_r$ for 1/5 and 1/2 slopes.

CHAPTER 5 COMPARISON WITH EXPERIMENTS

In this chapter, the comparisons of the numerical model with the experiments are shown. First, the measured and predicted cross-shore variations of $\overline{\eta}$, σ_η , $\overline{u}$ and σ_u for the 15 pairs of the two repeated tests for the 1/5 slope experiment are presented. Second, the permeability effects on $\overline{\eta}$, σ_η , $\overline{u}$ and σ_u as well as the sensitivities of the numerical model to the roller effect, the breaker ratio parameter and bottom friction factor on the porous slope are examined. Last, the measured wave runup statistics for the 1/5 and 1/2 slope experiments are compared with the results of the time-averaged probabilistic model.

5.1 CROSS-SHORE WAVE TRANSFORMATION

Fig. 4-8 - Fig. 4-13 indicate that Eqs. (13), (14) and (25) may be used to predict the wave runup heights $R_{1/3}$ and $R_{2\%}$ as well as the value of R for the specified exceedance probability P if the mean $\overline{\eta}_r$ and standard deviation σ_r of the shoreline fluctuations can be

predicted accurately by the numerical model based on Eqs. (1) - (12). For each of the 57 tests, the bottom profiles $z_b(x)$ and $z_p(x)$ and the measured values of T_p, $\overline{\eta}$ and σ_η at $x=0$ are specified as input to the numerical model. The output of the numerical model includes the cross-shore variations of the variables in Eqs. (1) – (10), the reflected wave height given by Eq. (11), and the values of $\overline{\eta}_r$ and σ_r in Eq. (12). The only empirical parameter calibrated here is the breaker ratio parameter γ in Eq. (10). Use is made of γ = 0.7 calibrated by Kobayashi et al. (2005) who compared the numerical model with the experiment in which the 1/5 permeable slope in Fig. 3-1 was replaced by a submerged porous breakwater. The increase of γ causes the landward shift of irregular wave breaking on the gently sloping beach. The calibration of γ is made by comparing the measured and computed cross-shore variations of $\overline{\eta}$, σ_η, $\overline{u}$ and σ_u. The overall agreement is good except for the 1/2 slope tests with T_p = 1.5 and 2.4 s. For these tests, γ = 0.8 is used to improve the agreement but the reason for this increase of γ is not clear. The other empirical parameters calibrated by Kobayashi et al. (2005) are the slope adjustment factor b=3 in Eq. (10), the bottom friction factor on the stone slope, $f_b = 0.01$ in Eq. (14), and the turbulent porous flow resistance factor $\beta_0 = 5$ in Eq. (8). These values are used here in the subsequent analysis without any additional calibration. In the following, the roller effect is not included to reduce the number of the empirical parameters except in Section 5.3.

Fig. 5-1 - Fig. 5-15 compare the measured and predicted cross-shore variations of $\overline{\eta}$, σ_η, $\overline{u}$ and σ_u and the bottom profiles $z_b(x)$ and $z_p(x)$ for the 15 pairs of the two repeated tests (runs 1 and 2) for the 1/5 slope experiment. The tests were repeatable, indicating the reliability of the data. The computed results in the region of small water depth above SWL are reproducible, implying the numerical stability in the region of numerical

difficulties. The numerical model slightly overpredicts the wave setup $\bar{\eta}$ near the shoreline. The agreement for σ_η is good partly because the measured σ_η did not vary much. The comparisons for $\bar{u}$ and σ_u are somewhat ambiguous because the computed u is the depth-averaged velocity but the measured u corresponded to the mid-depth elevation. The agreement for $\bar{u}$ is better than expected from the previous comparison for a submerged breakwater by Kobayashi et al. (2005). The standard deviation σ_u is overpredicted slightly. On the other hand, the comparisons with the 27 tests in the 1/2 slope experiment were presented in the report by Kearney and Kobayashi (2001) who used the earlier version of this numerical model by Johnson and Kobayashi (1998). The present numerical model has also been compared with the 27 tests and the agreement has been found to be very similar because the major improvement here is essentially limited to the region near the shoreline where η and u were not measured.

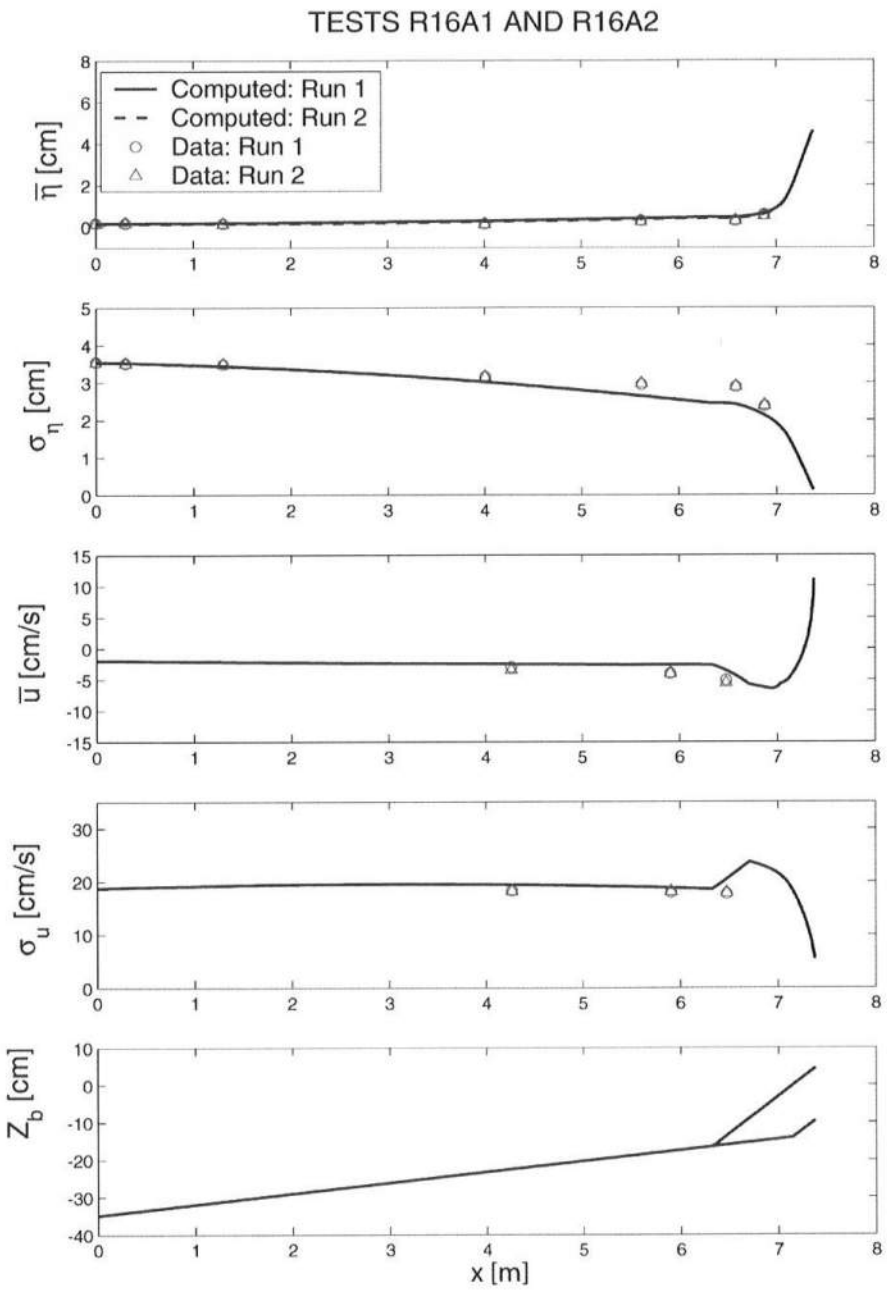

Fig. 5-1: Measured and predicted cross-shore variations of mean and standard deviation of η and u above bottom profile z_b for tests R16A1 and R16A2 on 1/5 slope.

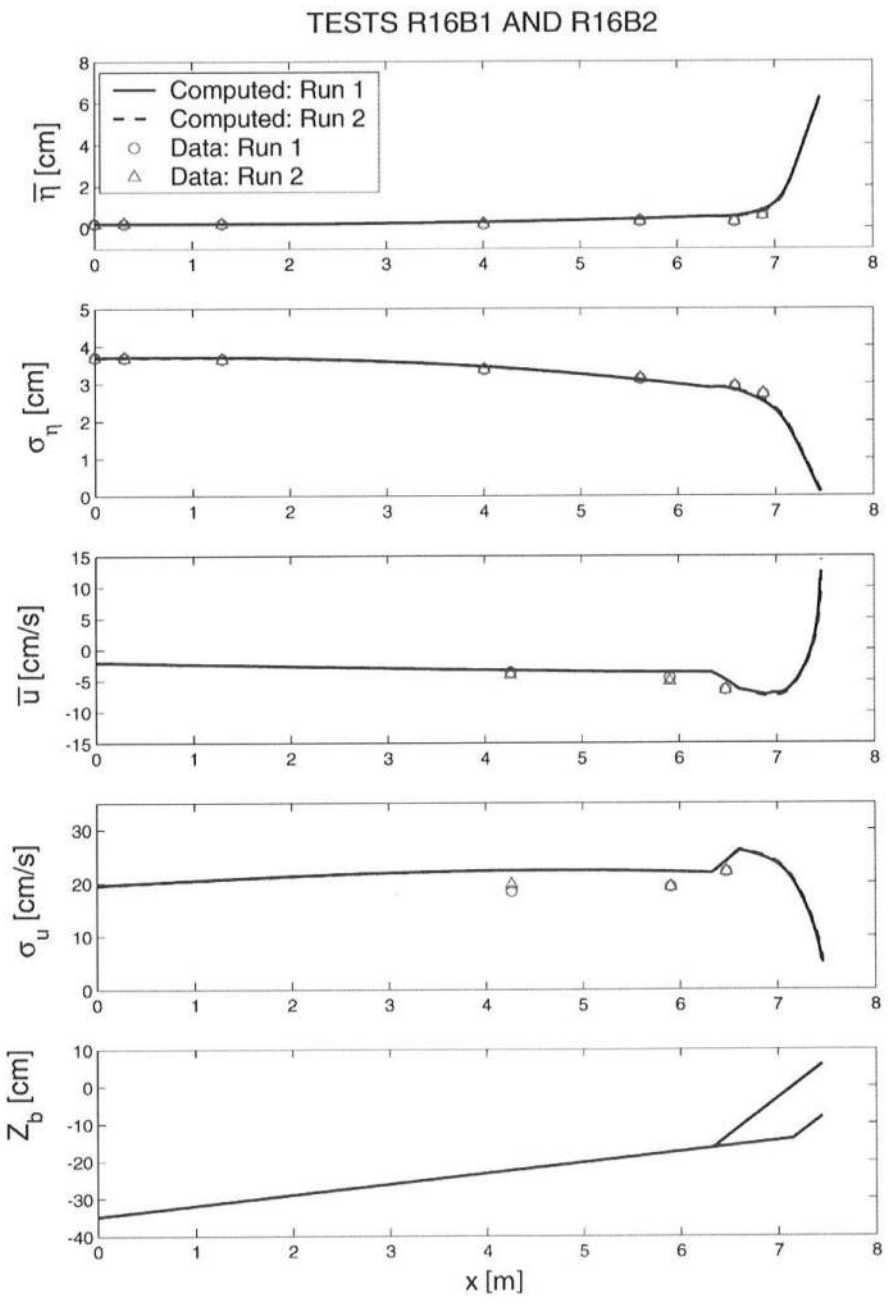

Fig. 5-2: Measured and predicted cross-shore variations of mean and standard deviation of η and u above bottom profile z_b for tests R16B1 and R16B2 on 1/5 slope.

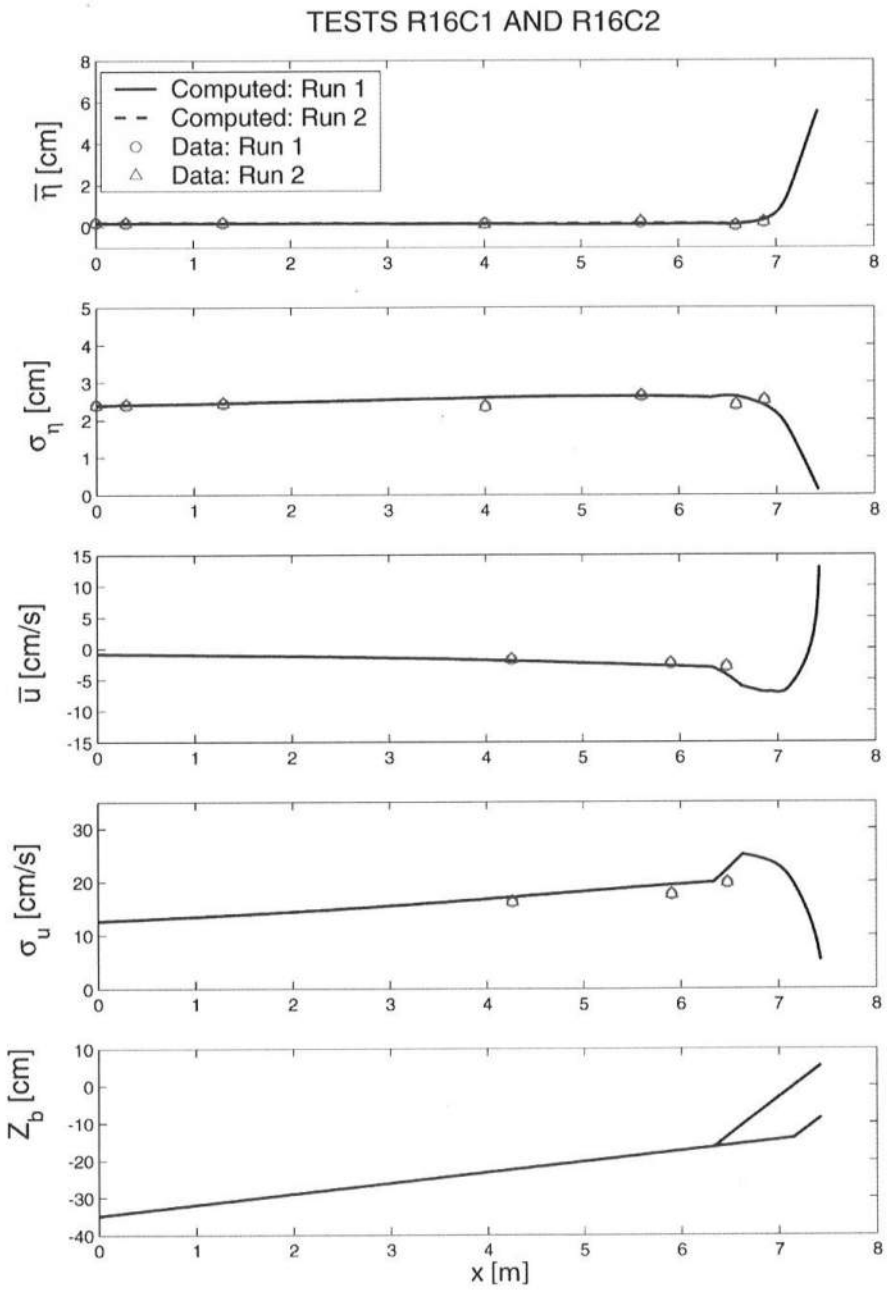

Fig. 5-3: Measured and predicted cross-shore variations of mean and standard deviation of η and u above bottom profile z_b for tests R16C1 and R16C2 on 1/5 slope.

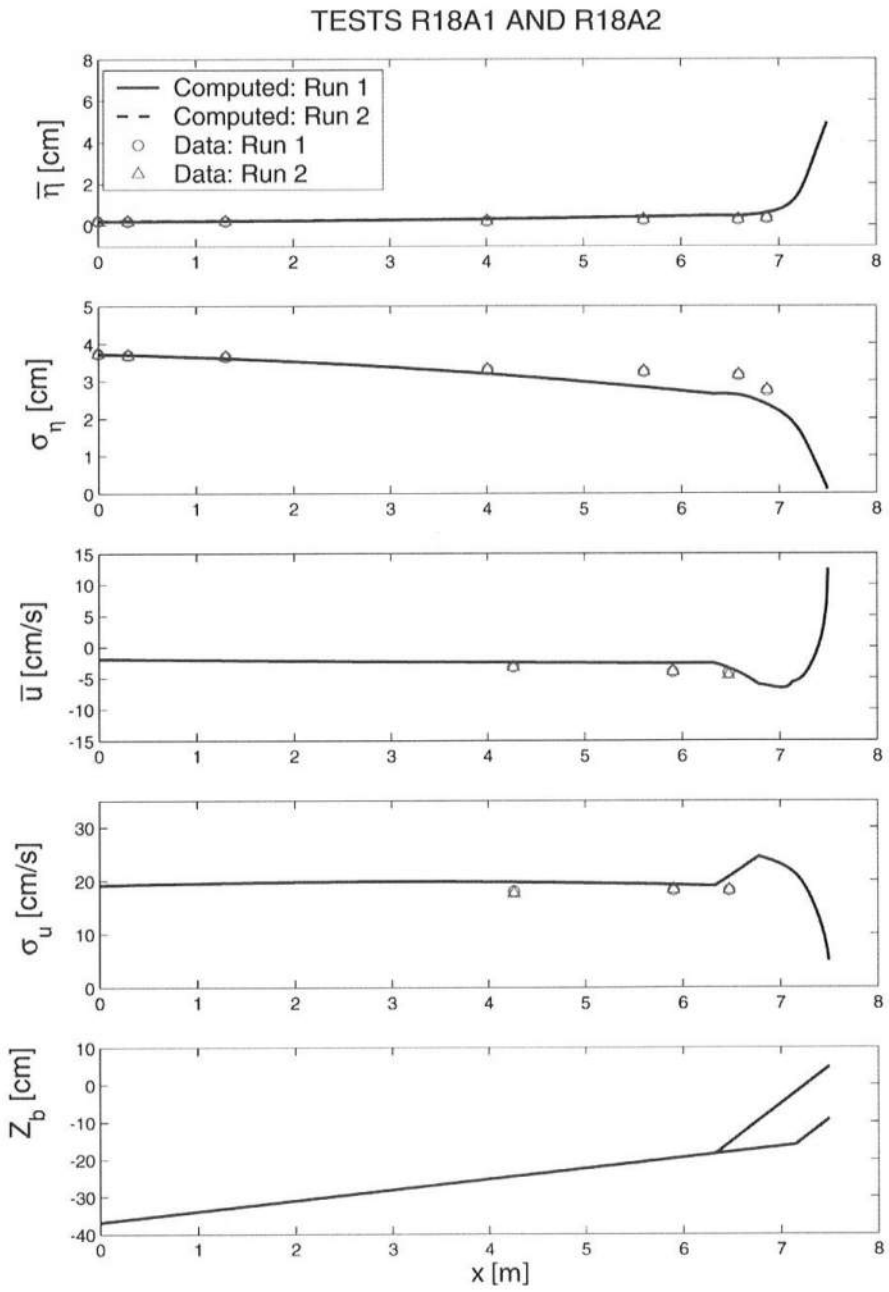

Fig. 5-4: Measured and predicted cross-shore variations of mean and standard deviation of η and u above bottom profile z_b for tests R18A1 and R18A2 on 1/5 slope.

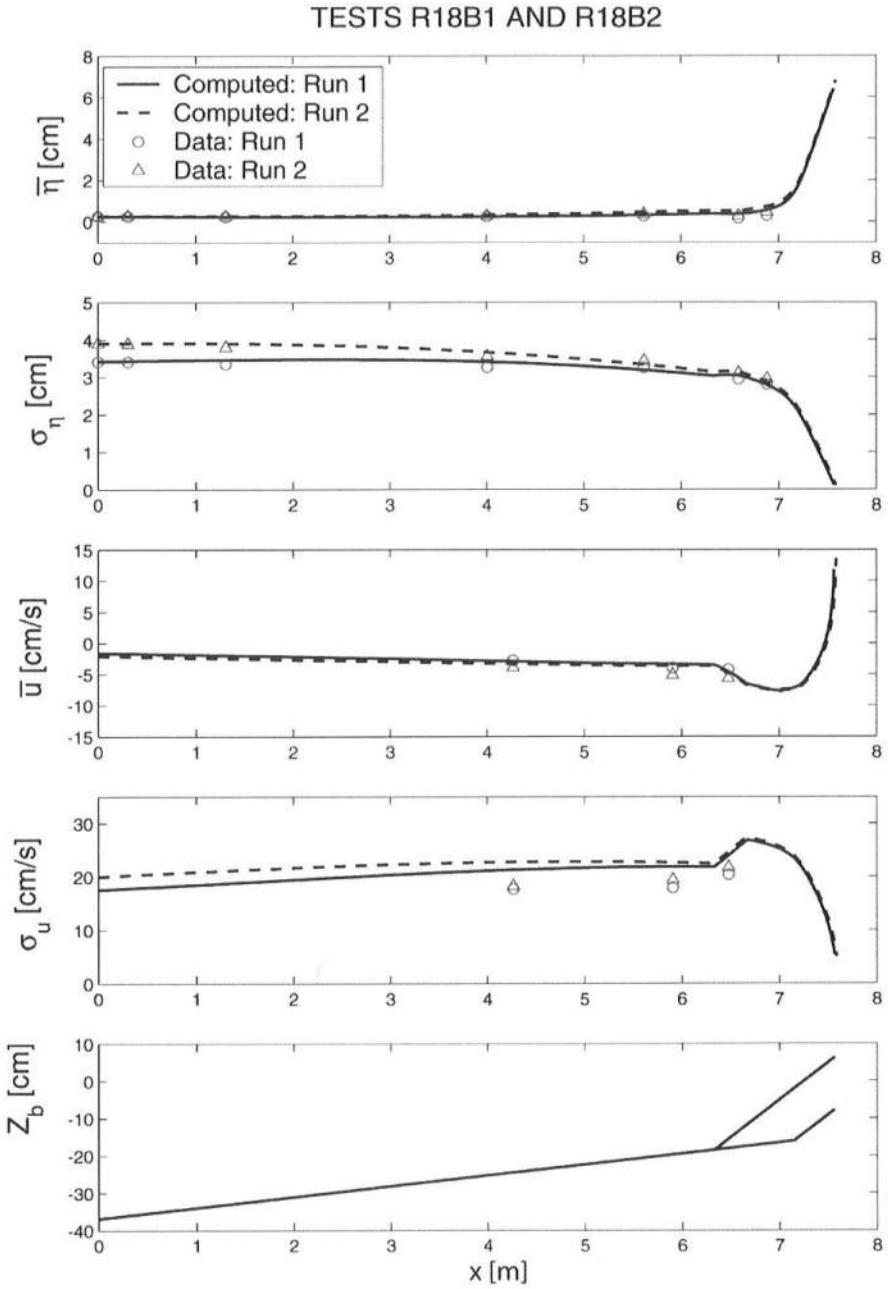

Fig. 5-5: Measured and predicted cross-shore variations of mean and standard deviation of η and u above bottom profile z_b for tests R18B1 and R18B2 on 1/5 slope.

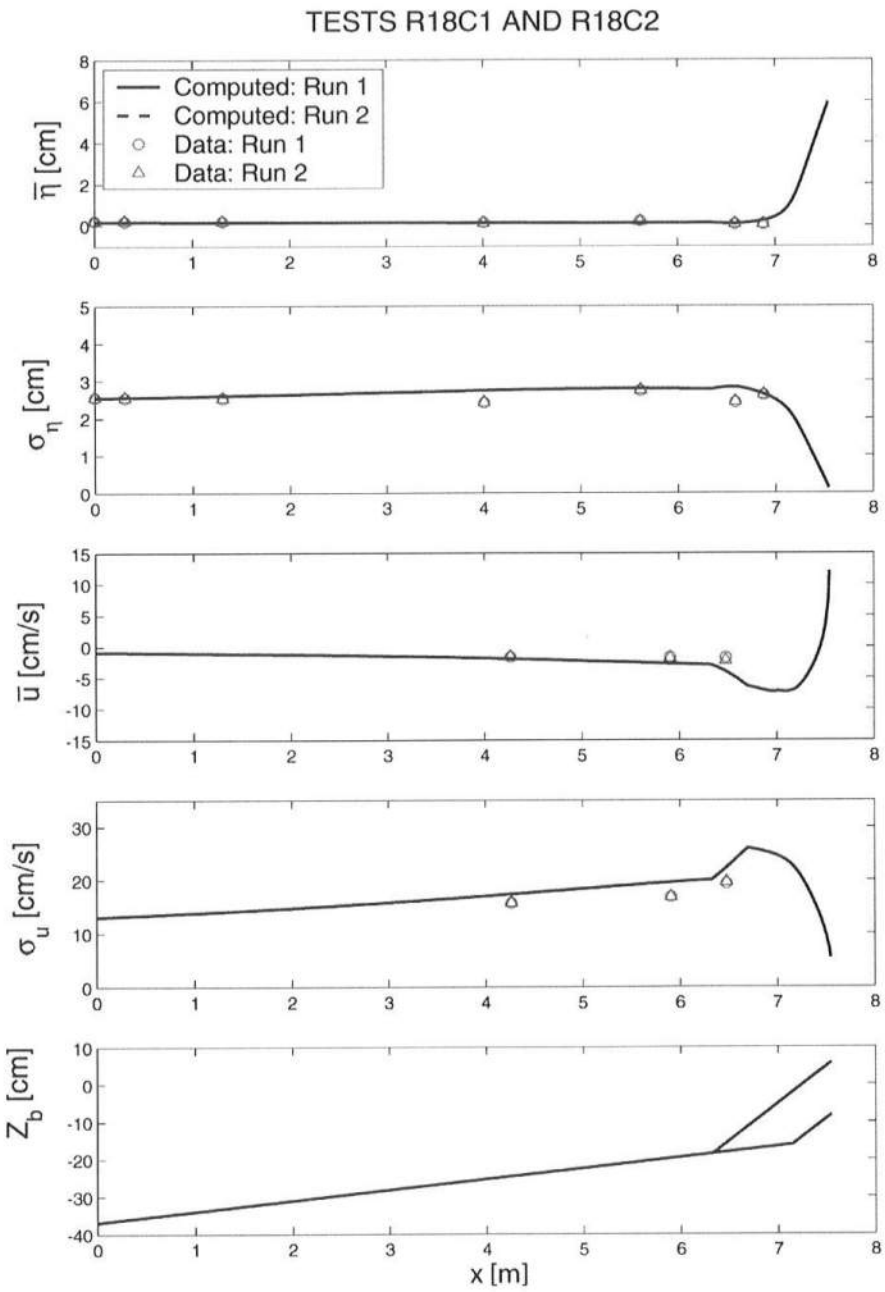

Fig. 5-6: Measured and predicted cross-shore variations of mean and standard deviation of η and u above bottom profile z_b for tests R18C1 and R18C2 on 1/5 slope.

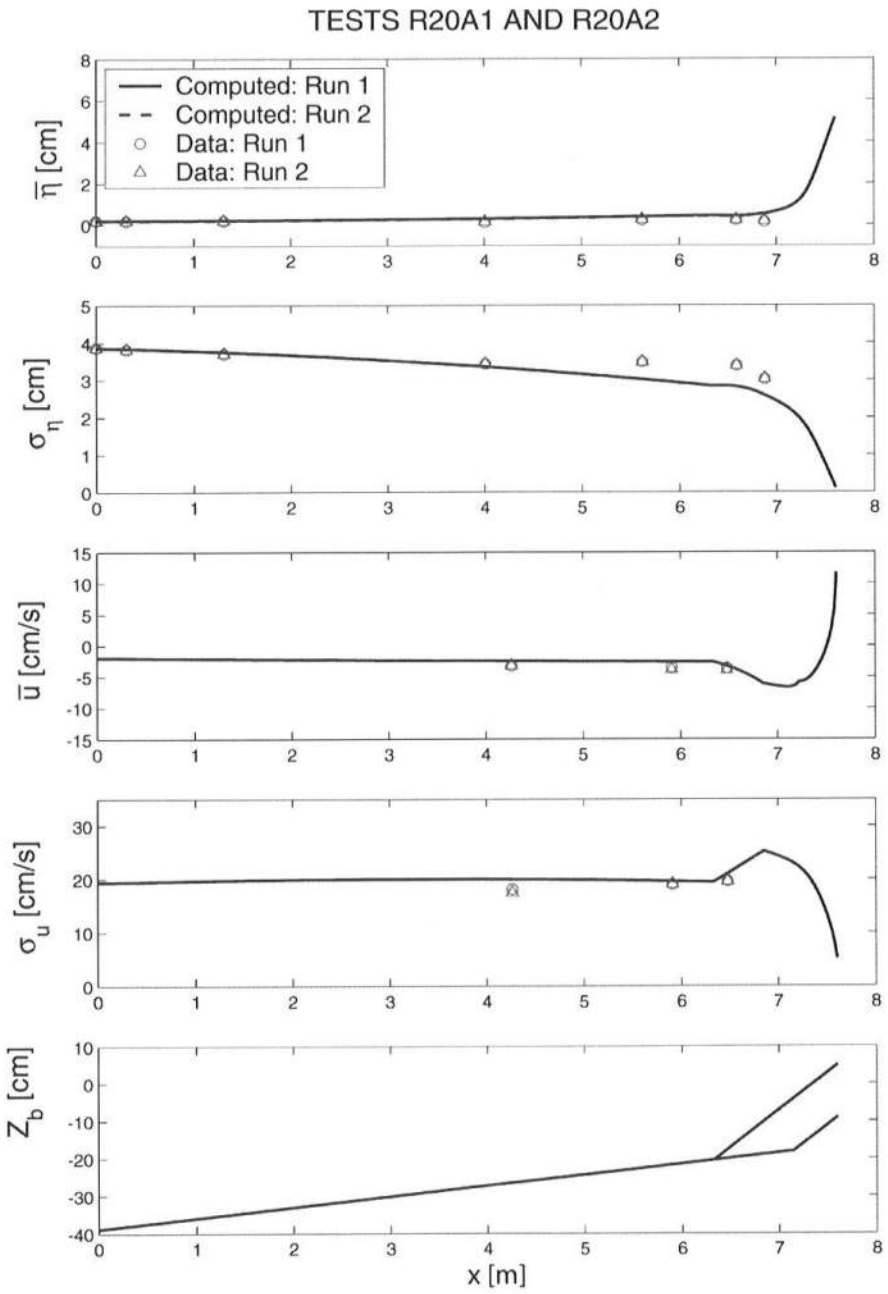

Fig. 5-7: Measured and predicted cross-shore variations of mean and standard deviation of η and u above bottom profile z_b for tests R20A1 and R20A2 on 1/5 slope.

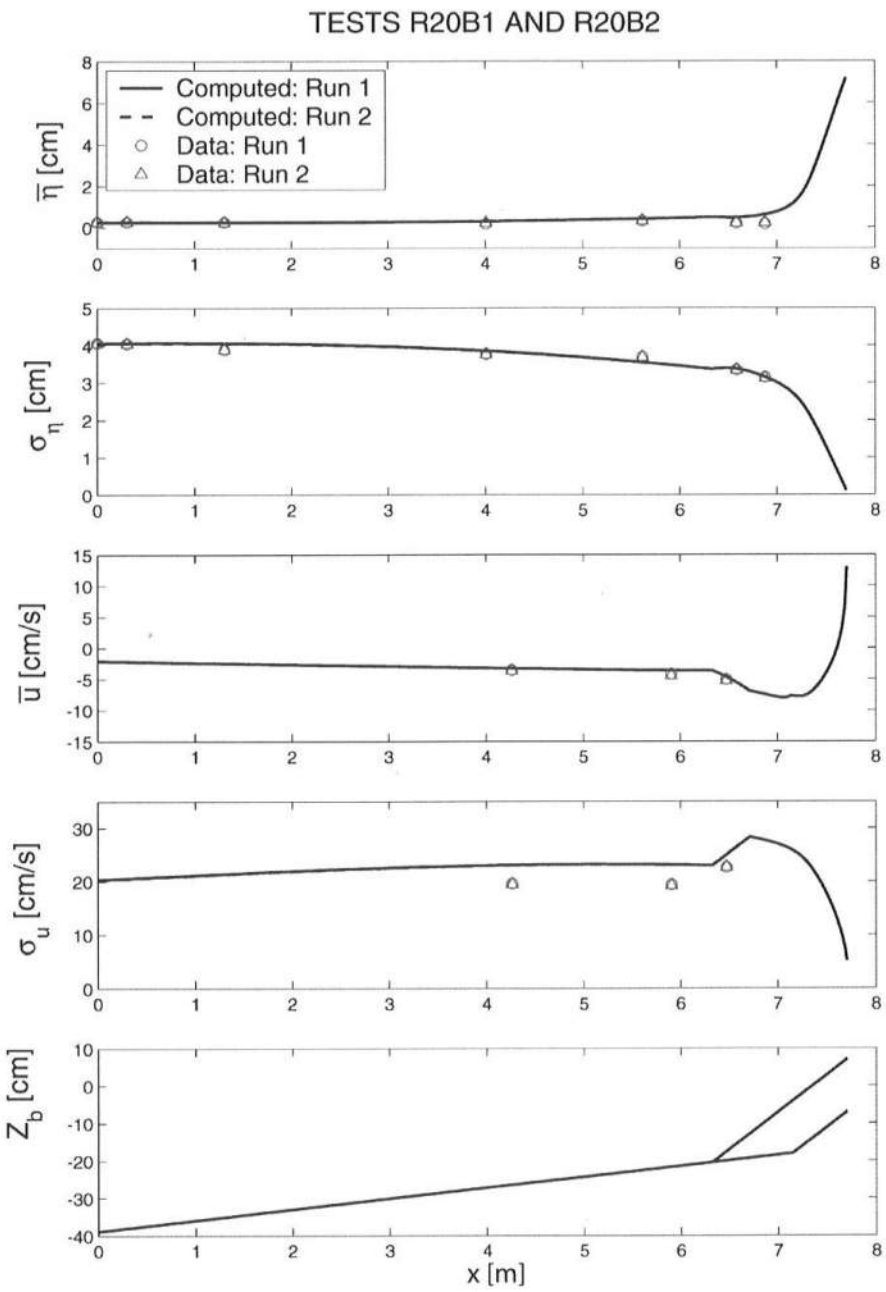

Fig. 5-8: Measured and predicted cross-shore variations of mean and standard deviation of η and u above bottom profile z_b for tests R20B1 and R20B2 on 1/5 slope.

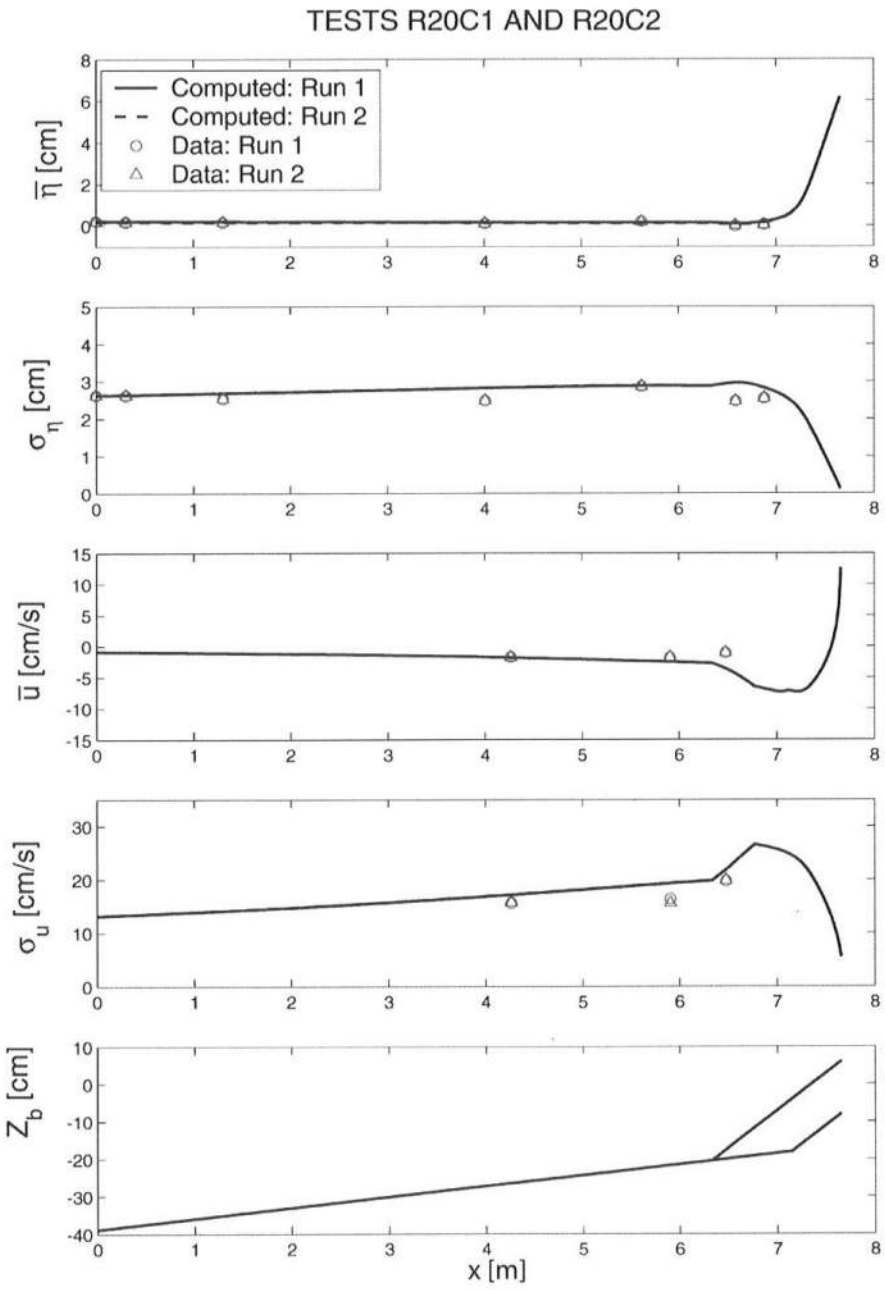

Fig. 5-9: Measured and predicted cross-shore variations of mean and standard deviation of η and u above bottom profile z_b for tests R20C1 and R20C2 on 1/5 slope.

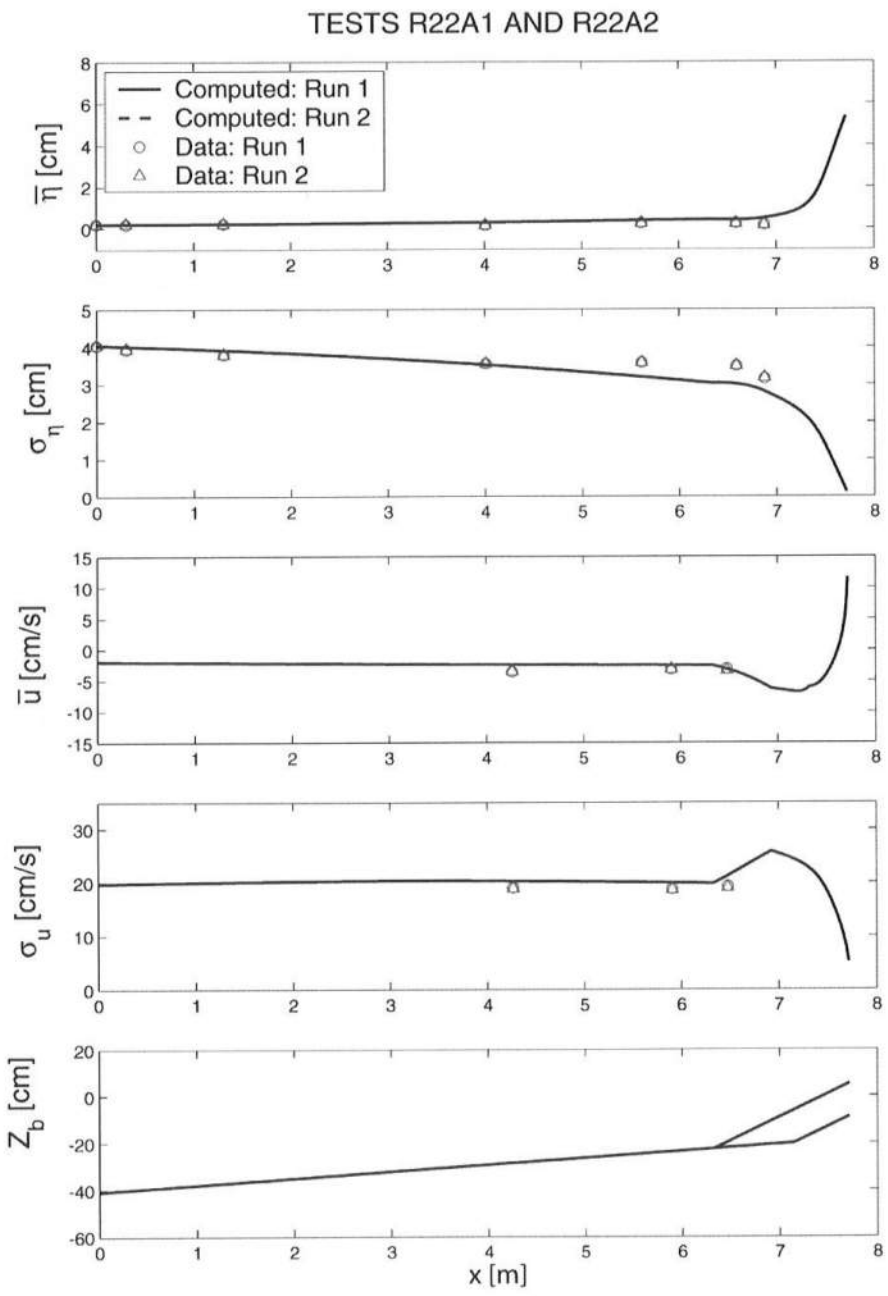

Fig. 5-10: Measured and predicted cross-shore variations of mean and standard deviation of η and u above bottom profile z_b for tests R22A1 and R22A2 on 1/5 slope.

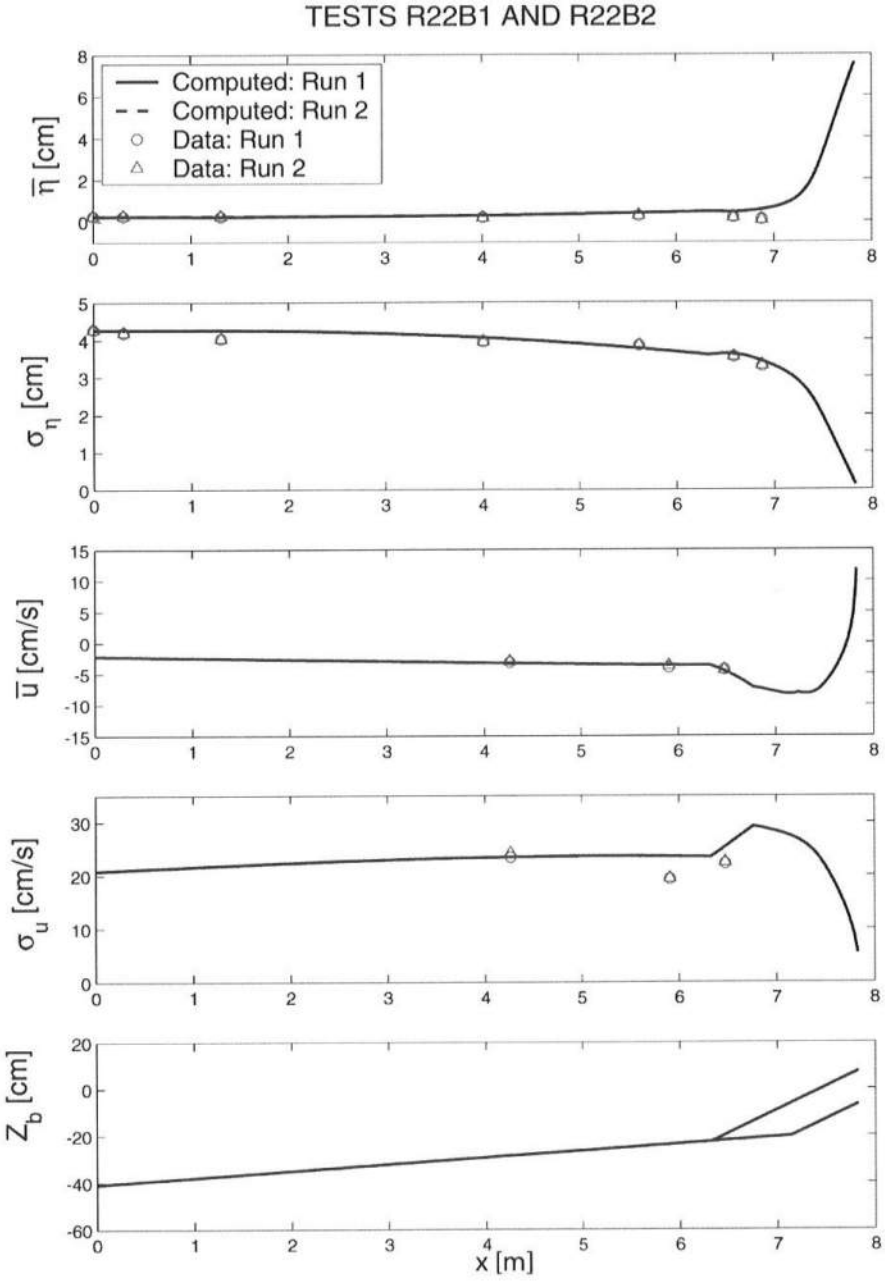

Fig. 5-11: Measured and predicted cross-shore variations of mean and standard deviation of η and u above bottom profile z_b for tests R22B1 and R22B2 on 1/5 slope.

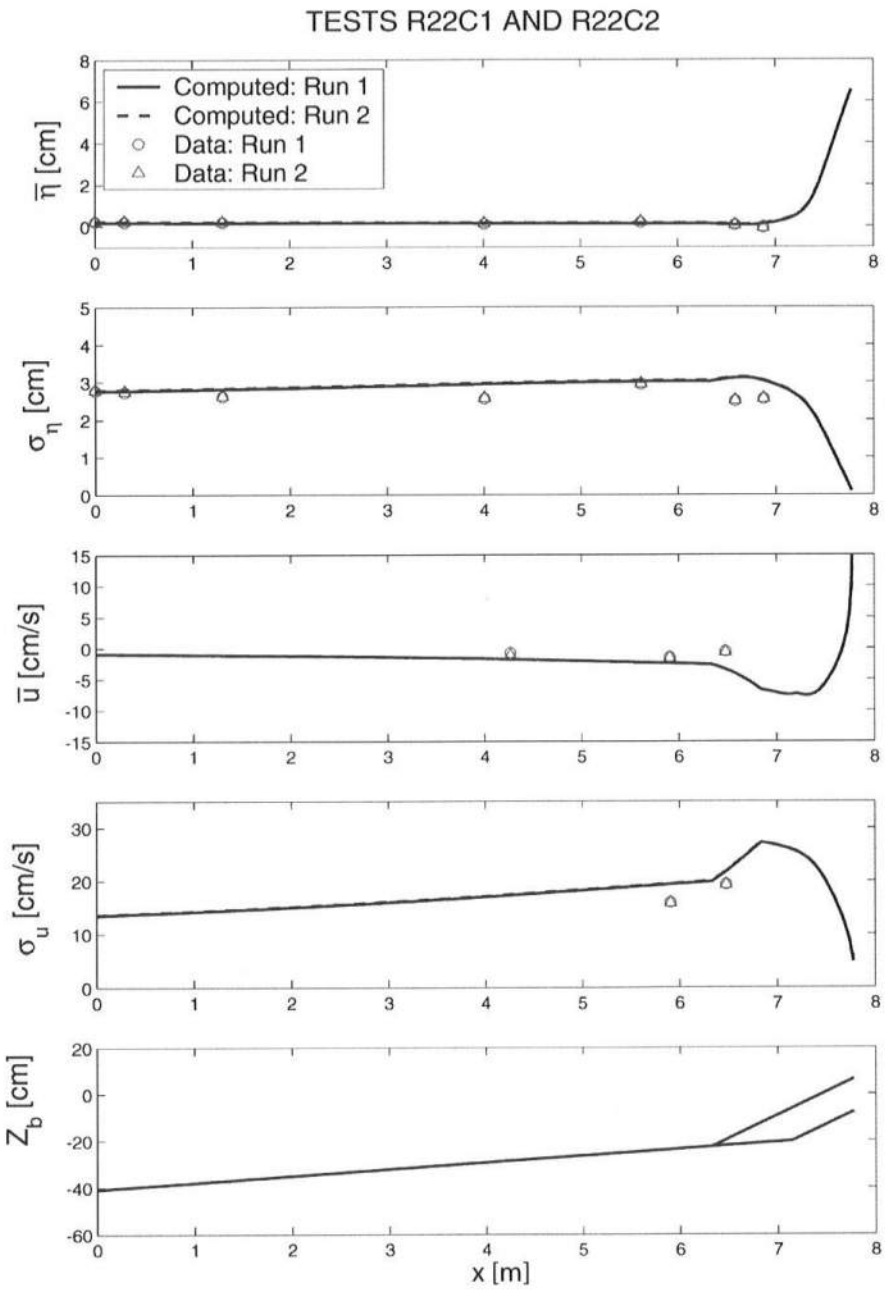

Fig. 5-12: Measured and predicted cross-shore variations of mean and standard deviation of η and u above bottom profile z_b for tests R22C1 and R22C2 on 1/5 slope where the measured σ_u by ADV1 was not reliable.

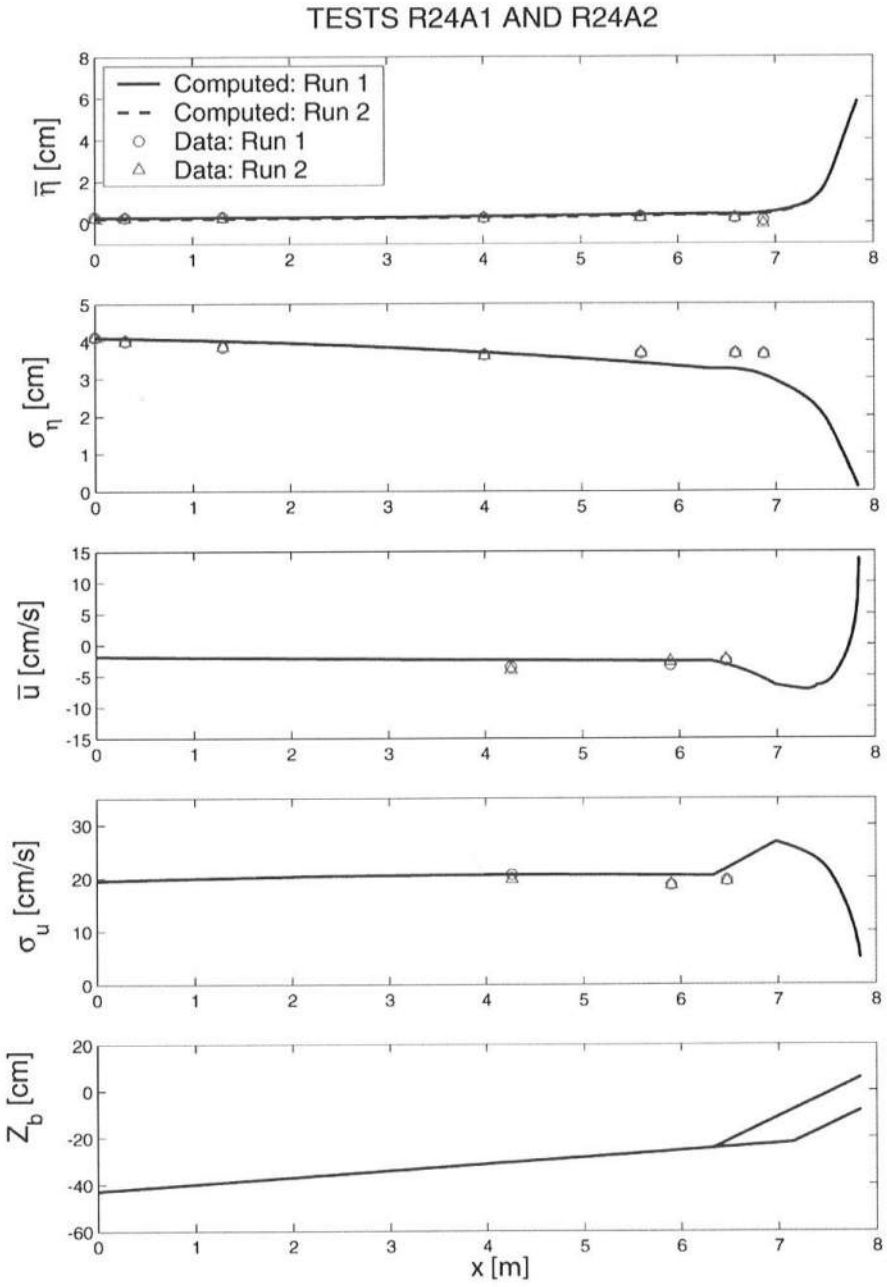

Fig. 5-13: Measured and predicted cross-shore variations of mean and standard deviation of η and u above bottom profile z_b for tests R24A1 and R24A2 on 1/5 slope.

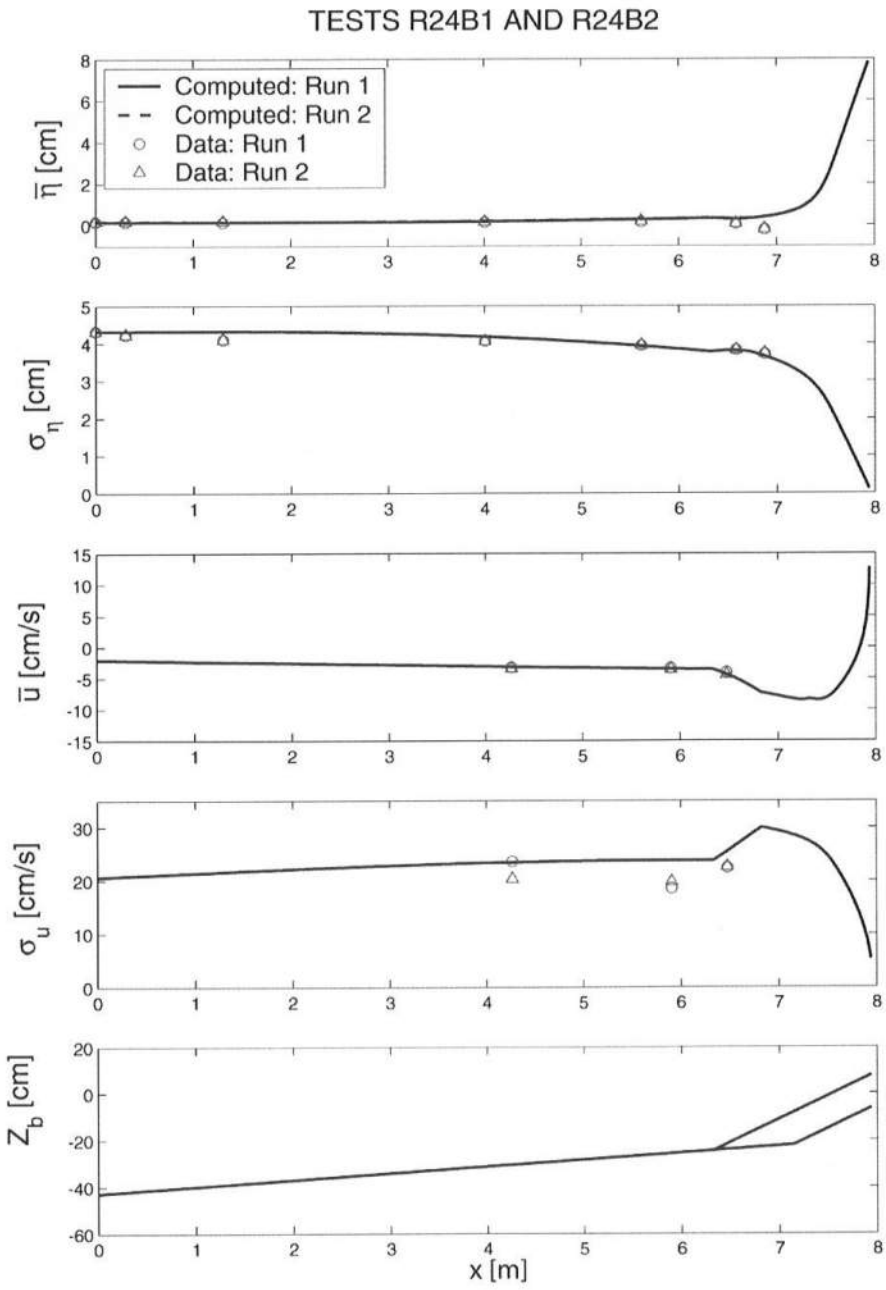

Fig. 5-14: Measured and predicted cross-shore variations of mean and standard deviation of η and u above bottom profile z_b for tests R24B1 and R24B2 on 1/5 slope.

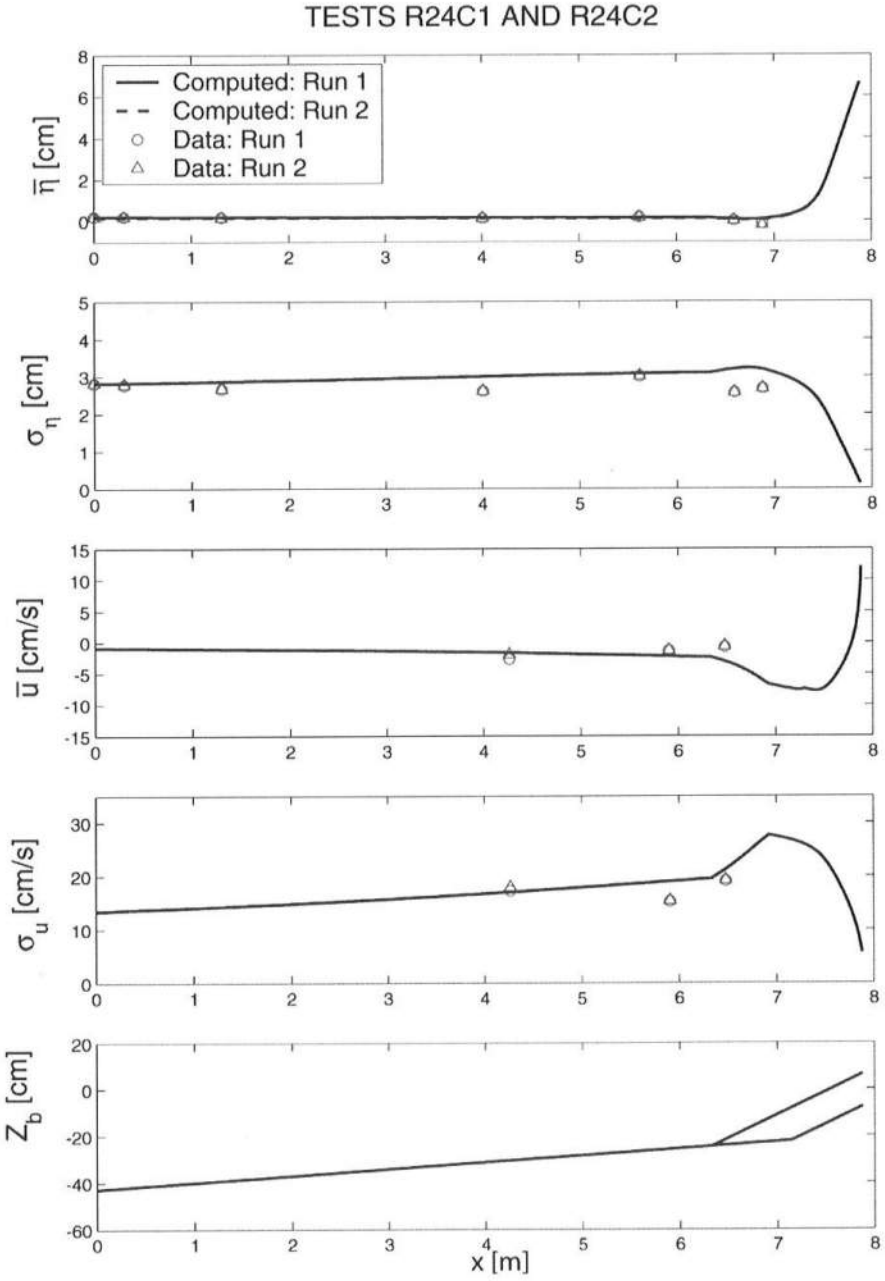

Fig. 5-15: Measured and predicted cross-shore variations of mean and standard deviation of η and u above bottom profile z_b for tests R24C1 and R24C2 on 1/5 slope.

5.2 EFFECTS OF POROUS LAYER

To examine the permeability effects on $\bar{\eta}, \sigma_\eta, \bar{u}$ and σ_u, computation is also made for the 1/5 slope tests with no permeable layer by specifying $z_p = z_b$ and $h_p = 0$ in Eqs. (6) and (7). The empirical parameters used in the computations are $\gamma = 0.7$, $\beta_o = 5$, $b = 3$ and $f_b = 0.01$. The permeability effects tend to increase with the increase of the toe depth d_t and with the decrease of the period T_p. Consequently, the computed results for the test with the largest d_t = 24.6 cm and the smallest T_p = 1.59 s are presented in Fig. 5-16 where H_{rms} = 11.59 cm at $x = 0$. The cross-shore variations above the 1/5 slope are shown to differentiate the computed variations on the porous and impermeable slopes. The wave setup $\bar{\eta}$ reaches a higher elevation as it approaches tangential to the impermeable slope. The standard deviation σ_η decreases landward more gradually because of no energy dissipation due to porous flow resistance. The return current $\bar{u}$ is negative (offshore) on the impermeable slope, whereas $\bar{u}$ becomes positive above the still water shoreline on the porous slope because of infiltration and return flow inside the porous layer. The computed mean discharge velocity $\bar{v}$ is of the order of – 0.3 cm/s and the corresponding standard deviation σ_v is about 1 cm/s as shown in Fig. 5-19. Obviously, $\bar{v}$ and σ_v are zero for the impermeable slope. The standard deviation σ_u of the horizontal velocity u above the slope is much larger than σ_v and decreases landward more gradually on the impermeable slope.

Fig. 5-17 shows the computed cross-shore variations of n, a, Q and σ_*. The ratio n between the group and phase velocities in Eq. (2) is almost unity in the shallow water on the 1/5 slope. The coefficient a in Eq. (10) increases landward with the decrease of $\bar{h}$ and significantly increases D_B due to intense wave breaking on the 1/5 slope. The fraction Q of

breaking waves in Eq. (10) increases rapidly over the 1/5 slope and indicates the breaking of all waves in the region $x > 6.9$ m. The ratio $\sigma_* = \sigma_\eta / \bar{h}$ increases landward but is less than unity due to the empirical adjustment for $\sigma_* > \sigma_{*_c} = \gamma / \sqrt{8}$ discussed below Eq. (10).

Fig. 5-18 shows the cross-shore variations of $S_{xx}^* = S_{xx} / \rho g$ and $\tau_b^* = \tau_b / \rho g$ involved in the momentum equation in Eq. (1). S_{xx} decreases rapidly due to wave breaking in the region of $Q = 1$ and causes the increase of the wave setup. τ_b is negative because $\bar{u} < 0$ except above the still water shoreline on the porous slope because of infiltration into the permeable layer. $|\tau_b|$ is somewhat larger on the impermeable slope due to the larger σ_u on the impermeable slope.

Fig. 5-20 shows the computed cross-shore variations of $F^* = F / \rho g$, $D_B^* = D_B / \rho g$, $D_r^* = D_r / \rho g$ and $D_f^* = D_f / \rho g$ involved in the energy equation in Eq. (1). The wave energy flux F decreases landward due to the energy dissipation but the difference between the values on the porous and impermeable slopes is small. This is because the energy dissipation rate D_B due to wave breaking increases on the impermeable slope for which the energy dissipation rate D_r due to porous flow resistance is zero. The energy dissipation rate D_f due to the bottom friction is of the order of 0.02 D_B. The computed results in Fig. 5-16 - Fig. 5-20 may not be very accurate but indicate the interconnected nature of the variables in Eqs. (1) – (10).

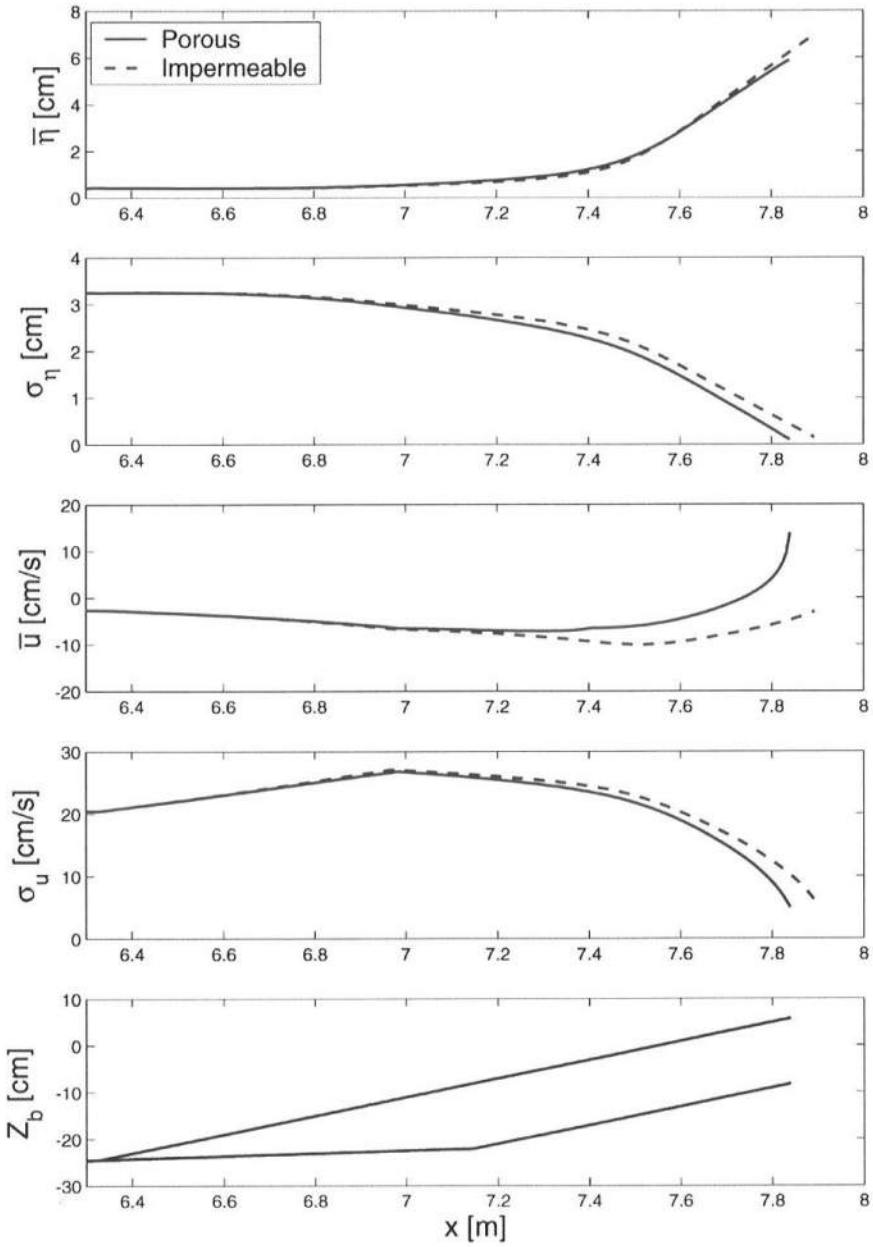

Fig. 5-16: Permeability effects on $\bar{\eta}, \sigma_\eta, \bar{u}$ and σ_u for test R24A1.

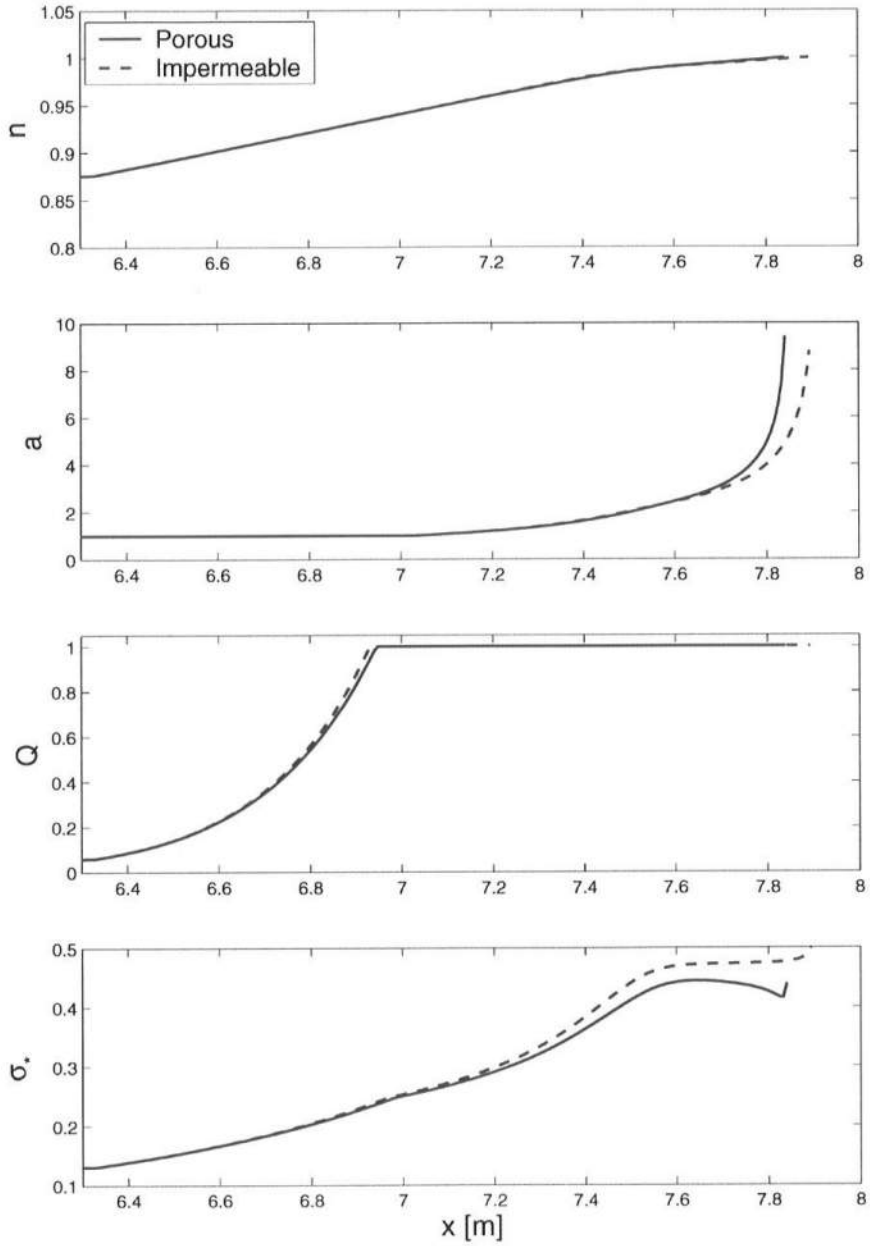

Fig. 5-17: Permeability effects on n, a, Q and σ_* for test R24A1.

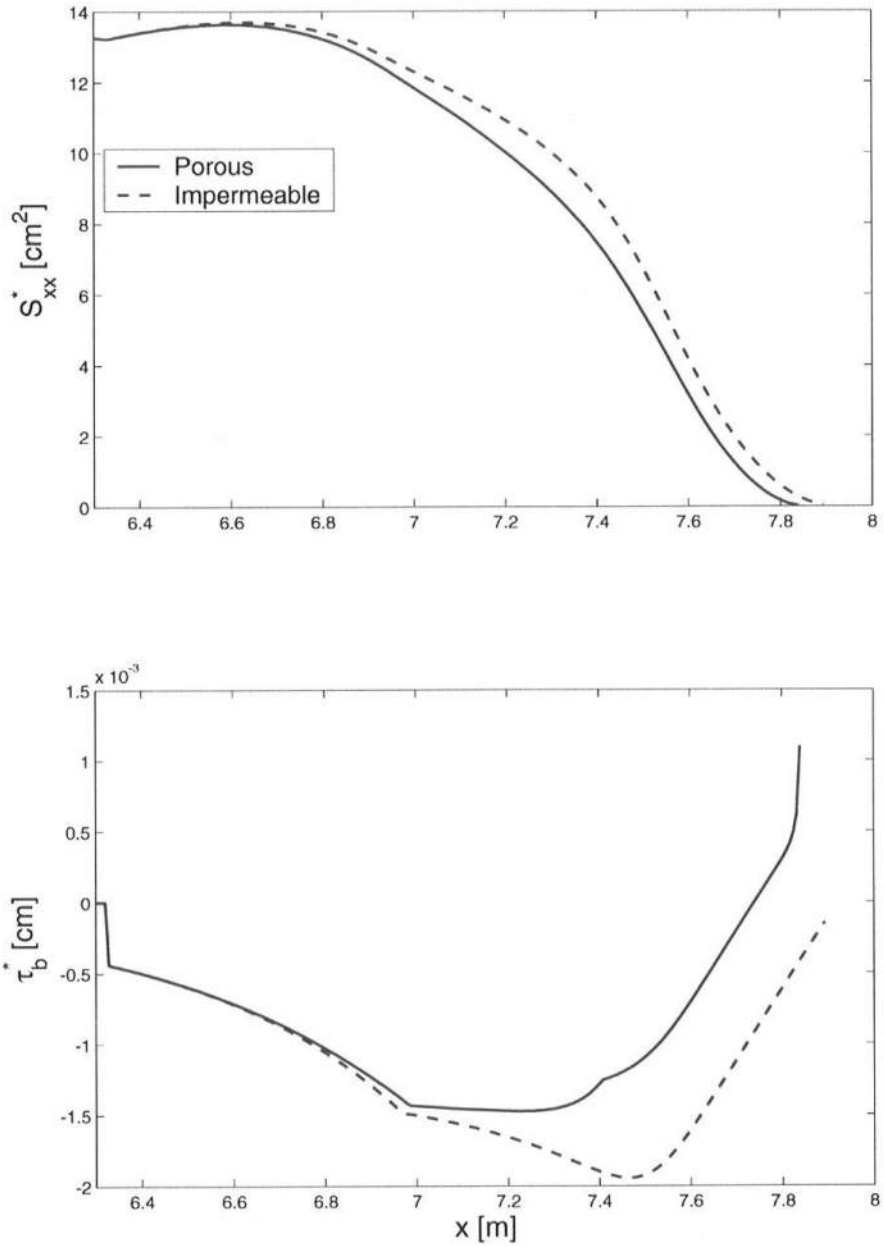

Fig. 5-18: Permeability effects on S^*_{xx} and τ^*_b for test R24A1.

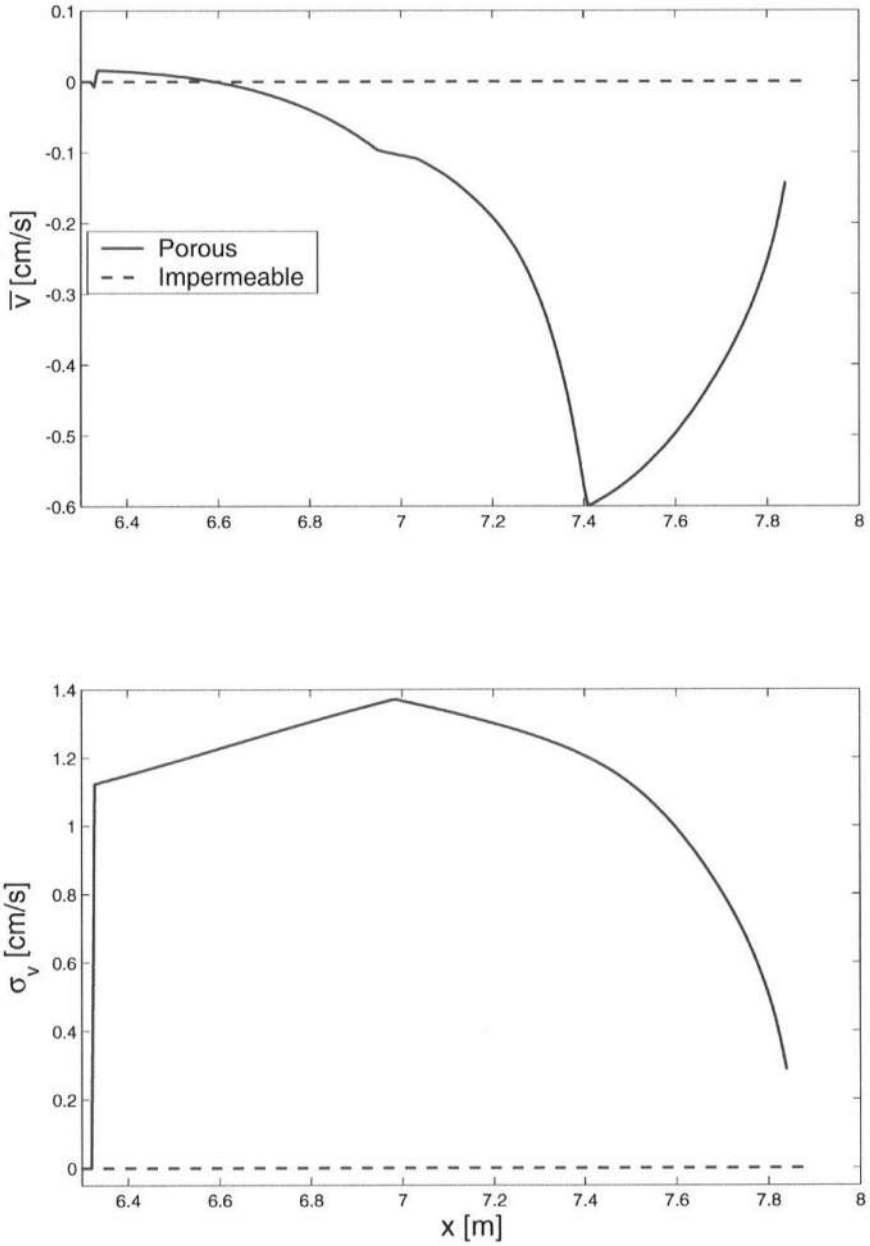

Fig. 5-19: Permeability effects on $\bar{v}$ and σ_v for test R24A1.

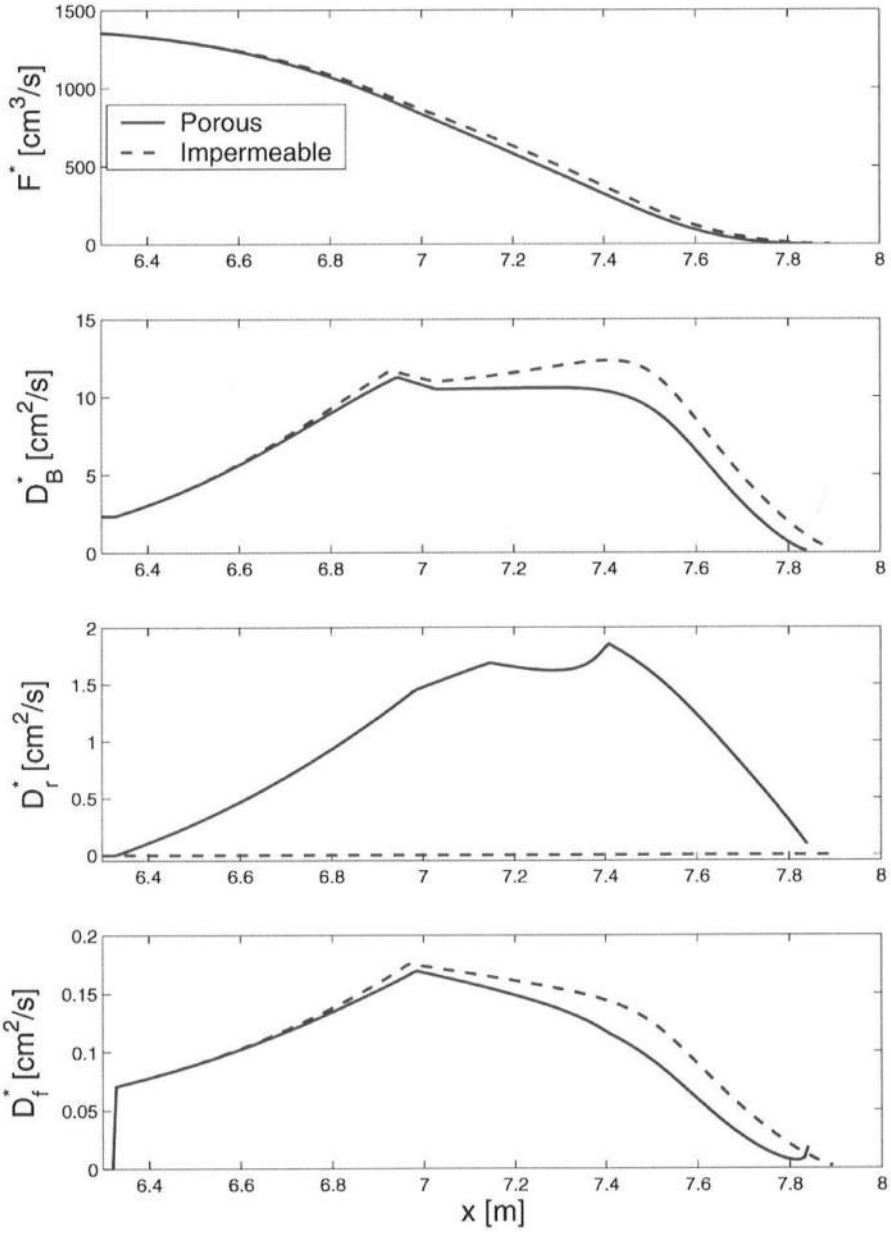

Fig. 5-20: Permeability effects on wave energy flux $F = \rho g F^*$ and dissipation rates $D_B = \rho g D_B^*$, $D_r = \rho g D_r^*$ and $D_f = \rho g D_f^*$ due to wave breaking, porous flow resistance, and bottom friction, respectively.

5.3 SENSITIVITY TO ROLLER EFFECT

In this section the sensitivity of the computed results to the roller effect is investigated. Fig. 5-21 shows the measured and computed $\overline{\eta}, \sigma_\eta, \overline{u}$ and σ_u for test R20B1 where IROLL = 1 and IROLL = 0 indicate the computed results with and without the roller volume flux q_r in Eqs. (2) and (6). The empirical parameters used in the computations are $\gamma = 0.7$, $\beta_o = 5$, $b = 3$ and $f_b = 0.01$. The inclusion of the roller volume flux q_r increases significantly the wave setup $\overline{\eta}$ near the still water shoreline, while the effect on $\overline{\eta}$ over the gentler impermeable beach slope is negligible. The standard deviations of the free surface elevation and horizontal velocity σ_η and σ_u decrease landward more gradually with IROLL = 1 near the still water shoreline where the wave energy flux $F = \rho g C_g \sigma_\eta^2$ in the adopted wave energy equation (1) has no effect of q_r. The mean horizontal velocity $\overline{u}$ becomes more negative (seaward), on the porous slope due to the contribution of the roller volume flux q_r in Eq. (6), whereas the onshore mean velocity $\overline{u}$ above the still water shoreline is reduced.

The inclusion of the roller effect with the additional empirical parameter β_r did not necessarily improve the agreement as was the case for sand beaches (Kobayashi et al., 2005). Consequently, the roller effect has been neglected for the rest of the computed results in this report.

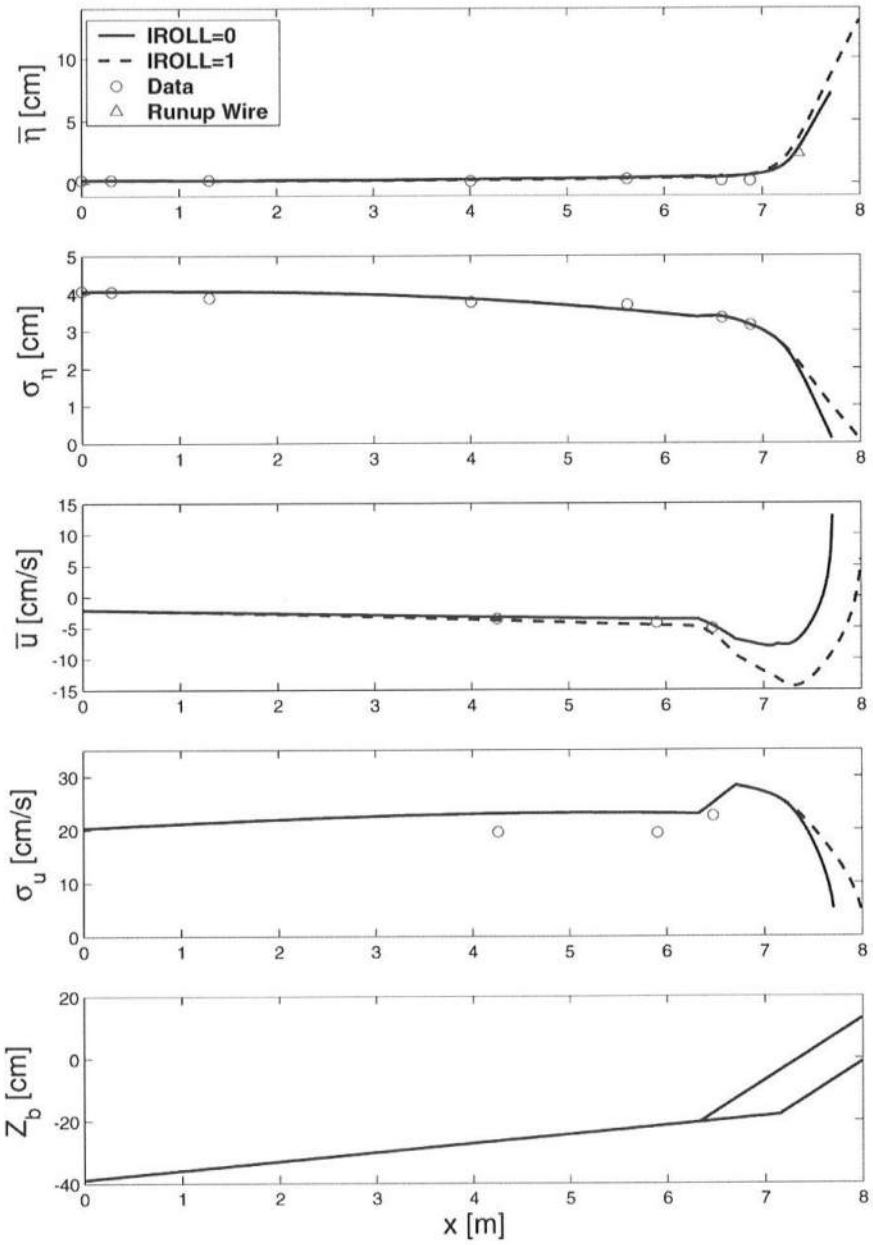

Fig. 5-21: Measured and computed $\bar{\eta}, \sigma_\eta, \bar{u}$ and σ_u for test R20B1 where IROLL = 0 and 1 indicate the computed results with and without the roller volume flux q_r.

5.4 SENSITIVITY TO BREAKER RATIO PARAMETER

The breaker ratio parameter γ in Eq. (10) is varied here to analyze the sensitivity of the computed results to this parameter. Table 6 shows the estimated values of the breaker ratio parameter γ using the empirical formula by Battjes and Stive (1985)

$$\gamma = 0.5 + 0.4 \tanh\left(33 s_o\right) \tag{26}$$

with $s_o = H_{rmso} / L_{op}$ = deep-water wave steepness. H_{rmso} and L_{op} are the equivalent deep water root-mean-square wave height and wavelength, respectively, based on linear wave shoaling for periodic waves with frequency $1/T_p$. The estimated values are in the range of 0.6 - 0.8 for all the 1/5 slope tests. Consequently, computations are made with $\gamma = 0.6, 0.7$ and 0.8. Fig. 5-22 shows the comparisons between the measured and computed $\overline{\eta}, \sigma_\eta, \overline{u}$ and σ_u for test R20B1 for $\gamma = 0.6, 0.7$ and 0.8. The decrease of γ reduces the depth-limited wave height H_m in Eq. (10), and increases Q and D_B in Eq. (10). This increase of D_B in Eq. (1) results in the decrease of σ_η, $\left|\overline{u}\right|$ and σ_u and the increase of $\overline{\eta}$ on the impermeable beach. However, $\overline{\eta}$ is reduced slightly on the permeable 1/5 slope due to the decrease of σ_η. As a whole, $\gamma = 0.7$ predicts σ_η better for most of the 1/5 slope tests and $\gamma = 0.7$ is used for all the 1/5 slope tests.

Table 6: Estimated breaker ratio parameter γ using Battjes and Stive (1985).

Test	H_{rms} [m]	d_1 [m]	T_p [s]	s_o	γ
R16A1	0.100	0.349	1.5	0.029	0.80
R16B1	0.105	0.349	2.3	0.012	0.65
R16C1	0.068	0.349	3.0	0.004	0.56
R18A1	0.105	0.369	1.5	0.031	0.81
R18B1	0.097	0.369	2.3	0.011	0.64
R18C1	0.072	0.369	3.0	0.005	0.56
R20A1	0.109	0.389	1.5	0.032	0.81
R20B1	0.115	0.389	2.3	0.013	0.67
R20C1	0.074	0.389	3.0	0.005	0.56
R22A1	0.114	0.409	1.5	0.034	0.82
R22B1	0.121	0.409	2.3	0.014	0.67
R22C1	0.078	0.409	3.0	0.005	0.57
R24A1	0.116	0.429	1.5	0.034	0.83
R24B1	0.122	0.429	2.3	0.014	0.68
R24C1	0.080	0.429	3.0	0.005	0.57

H_{rms} = measured root-mean-square wave height at wave gauge 1; d_1 = water depth at wave gauge 1; T_p = peak period; s_o = deep water steepness; γ = breaker ratio parameter

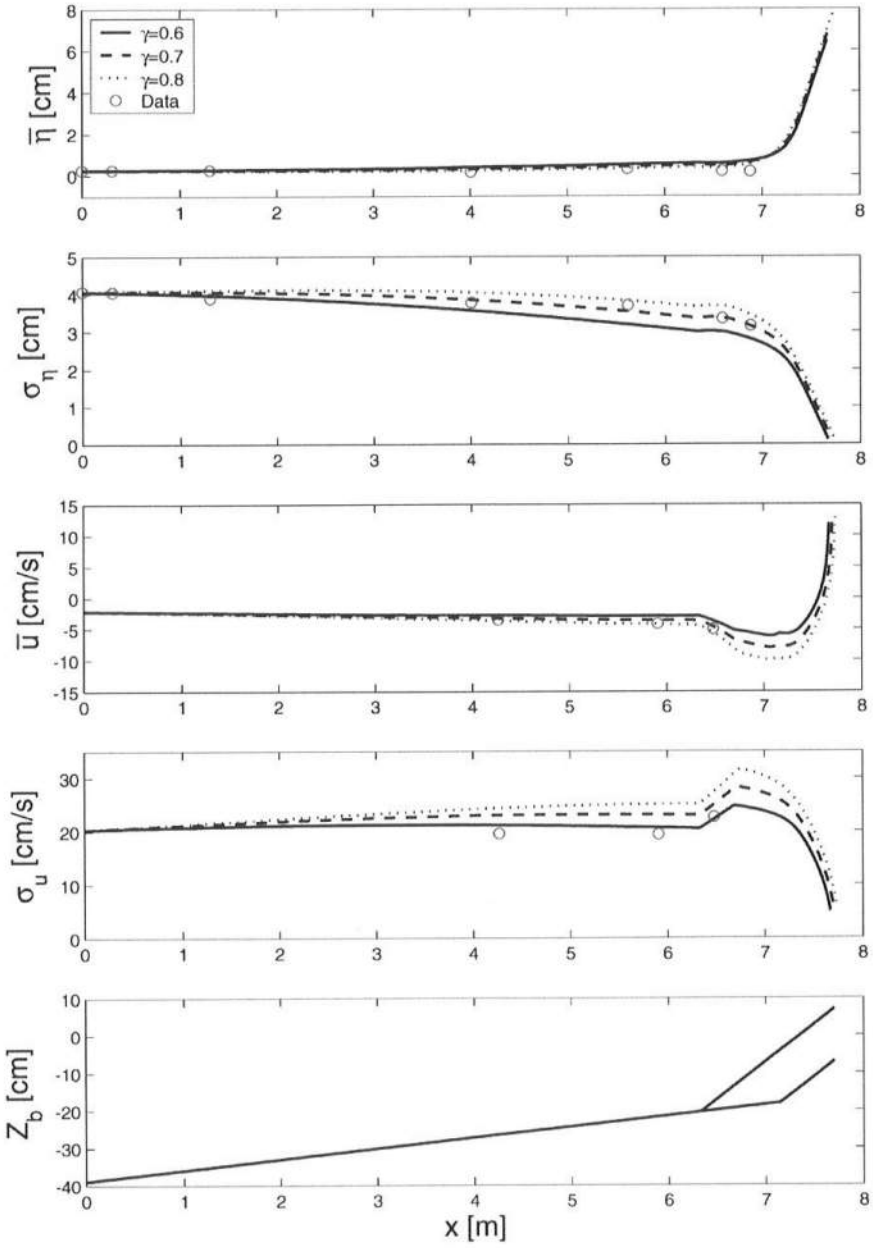

Fig. 5-22: Sensitivity to breaker ratio parameter $\gamma = 0.6, 0.7$ and 0.8 for test R20B1.

5.5 SENSITIVITY TO BOTTOM FRICTION FACTOR

The bottom friction factor f_b in Eq. (4) is varied to examine the sensitivity of the computed results to this parameter. Fig. 5-23 shows the measured and computed $\overline{\eta}, \sigma_\eta, \overline{u}$ and σ_u for the bottom friction factor $f_b = 0.01$ and 0.05 on the porous slope for test R20B1. The computed results by this time-averaged model are found to be insensitive to f_b, mainly because wave breaking and porous flow resistance are dominant in contrast to bottom friction on the 1/5 porous slope.

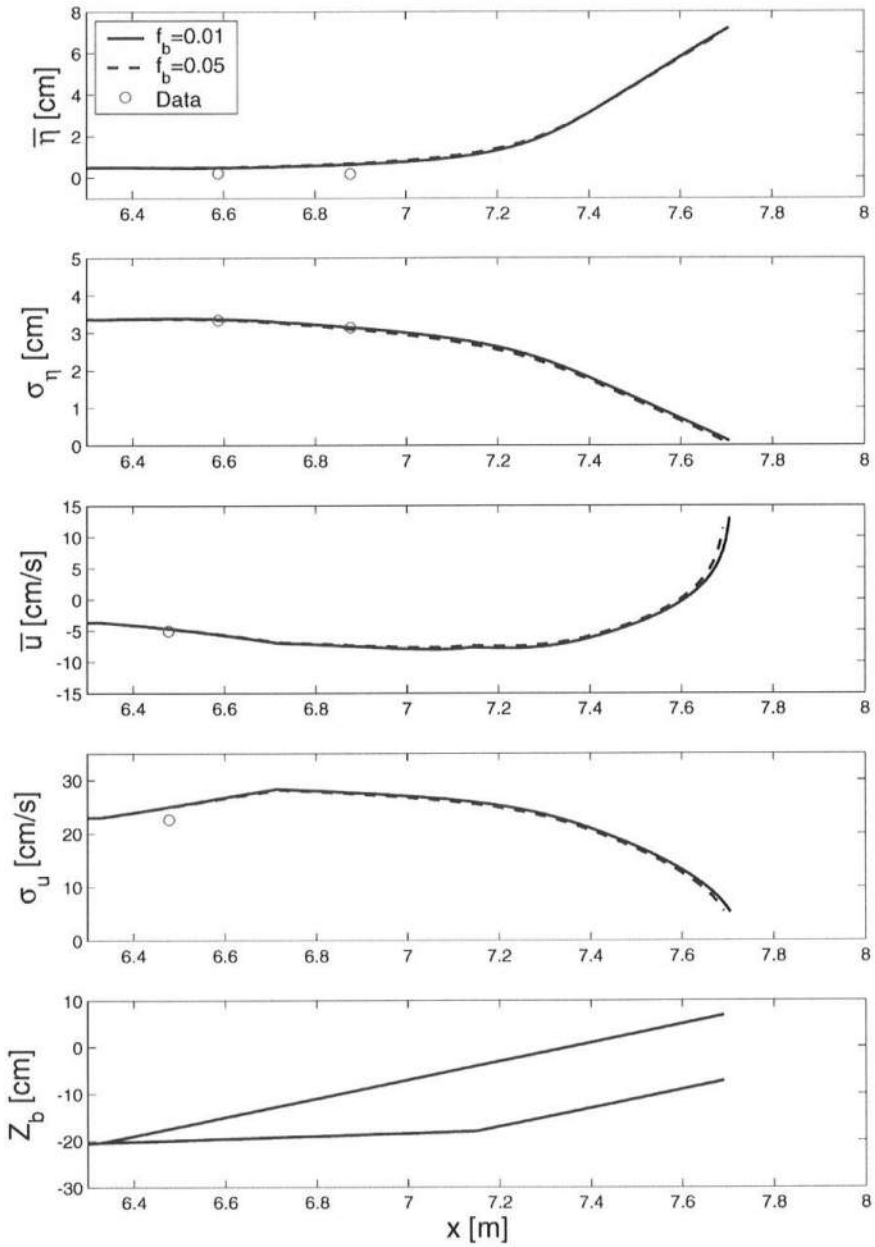

Fig. 5-23: Sensitivity to bottom friction factor $f_b = 0.01$ and 0.05 on the porous slope for test R20B1.

5.6 WAVE RUNUP STATISTICS

Fig. 5-24 and Fig. 5-25 compare the measured and predicted values of the mean $\overline{\eta}_r$ of the shoreline elevation η_r for the 1/5 and 1/2 slope experiments, respectively, for the different values of T_p. Fig. 5-26 and Fig. 5-27 compare the standard deviation σ_r for both experiments. The agreement is fair except for $\overline{\eta}_r$ on the 1/2 slope. The computed $\overline{\eta}_r$ for T_p = 2.4 and 4.7 s is too large in comparison with the measured $\overline{\eta}_r$ of about 1 cm. The effect of this overprediction on $R_{1/3}$ and $R_{2\%}$ is minor because σ_r on the 1/2 slope for T_p = 2.4 and 4.7 s is of the order of 4 cm and much larger than the measured $\overline{\eta}_r$.

Fig. 5-28 and Fig. 5-29 compare the measured and predicted significant runup heights $R_{1/3}$ for the 1/5 and 1/2 porous slope experiments for the different values of T_p, where $R_{1/3}$ is predicted using Eq. (14). The numerical model predicts $R_{1/3}$ within the error of about 20% partly because the slope correction is included in Eq. (14) empirically.

Fig. 5-30 and Fig. 5-31 compare the measured and predicted 2% runup heights $R_{2\%}$ where use is made of Eq. (25). The empirical formula of van der Meer and Janssen (1995) is also compared with the data. For the case of normally incident waves on a slope with no berm, this formula can be expressed as

$$R_{2\%} = 1.5\xi\gamma_f\gamma_h H_{1/3} \qquad \text{with} \qquad \xi \le 2 \tag{27}$$

with

$$\xi = \left(\frac{gT_p^2}{2\pi H_{1/3}}\right)^{0.5} \tan\theta \quad ; \quad \gamma_h = 1 - 0.03\left(4 - \frac{d_t}{H_{1/3}}\right)^2 \quad \text{if} \quad \frac{d_t}{H_{1/3}} < 4 \tag{28}$$

where ξ = surf similarity parameter; $H_{1/3}$ = significant wave height at the toe of the slope; γ_f = reduction factor due to slope roughness; γ_h = reduction factor due to wave breaking on a shallow foreshore which is less than unity if $(d_t / H_{1/3}) < 4$. Eq. (27) implies that (1.5 ξ) is replaced by 3.0 if $\xi > 2$. The reduction factor γ_h based on the measured ratio, $H_{2\%} / (1.4 H_{1/3})$, on a foreshore slope of 1/100 with $H_{2\%}$ = 2% wave height is assumed to be valid for the present beach slopes of 1/34.4 and 1/32.1. The reduction factor γ_f for a rubble layer with two or more stone diameter thickness was suggested to be in the range of 0.50 – 0.55 for $\xi < 4$ and larger for $\xi > 4$ but γ_f = 0.52 is used here to obtain the fair agreement shown in Fig. 5-30 and Fig. 5-31. The significant wave height $H_{1/3}$ for each test is obtained from the time series of the free surface elevation measured by the wave gauge at the toe of the slope. For the 1/5 slope tests, 0.97 $< \xi <$ 2.23 and 0.78 $< \gamma_h <$ 0.91. For the 1/2 slope tests, 2.85 $< \xi <$ 9.33 and 0.61 $< \gamma_h <$ 0.86. Eq. (27) developed originally for $0.5 < \xi < 5$ is applied here for $0.97 < \xi < 9.33$. All the parameters for the 1/5 and 1/2 slope experiments are summarized in Table 7 and Table 8. Fig. 5-30 and Fig. 5-31 indicate that the numerical model and empirical formula predicts $R_{2\%}$ within the error of about 20%. It should be noted that the numerical model uses the measured H_{rms} outside the surf zone instead of the measured $H_{1/3}$ at the toe of the slope.

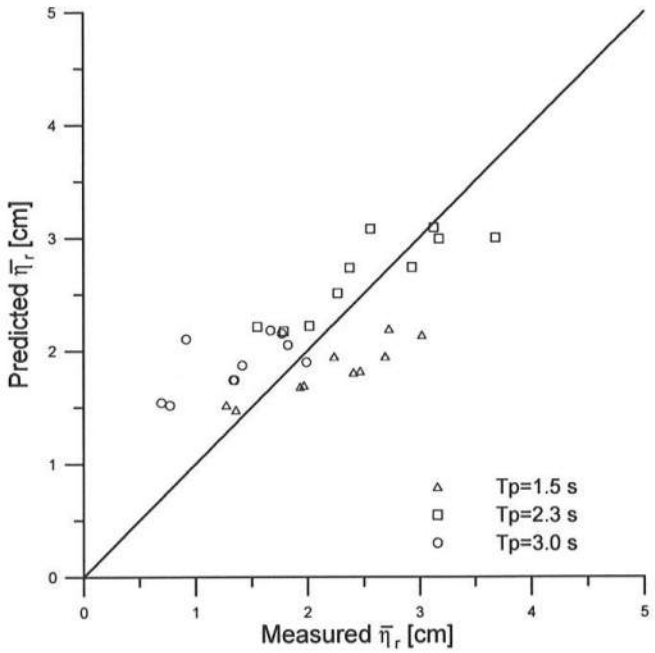

Fig. 5-24: Measured and predicted mean shoreline elevations $\overline{\eta_r}$ for 1/5 slope tests.

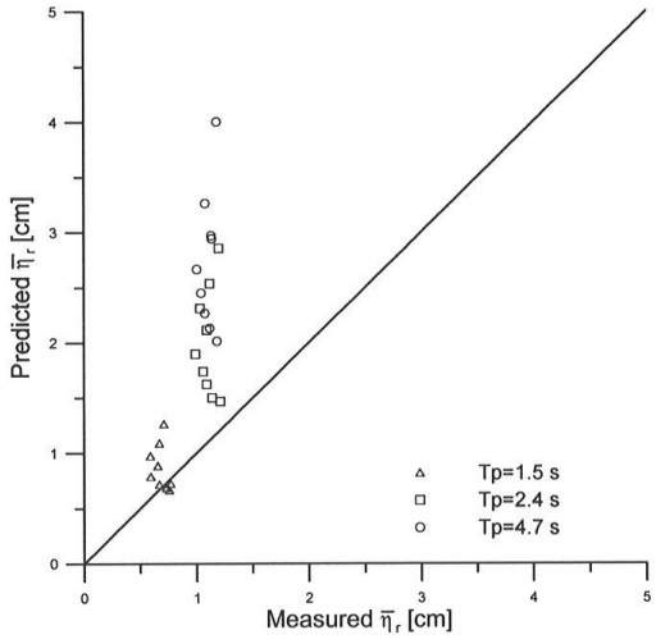

Fig. 5-25: Measured and predicted mean shoreline elevations $\overline{\eta_r}$ for 1/2 slope tests.

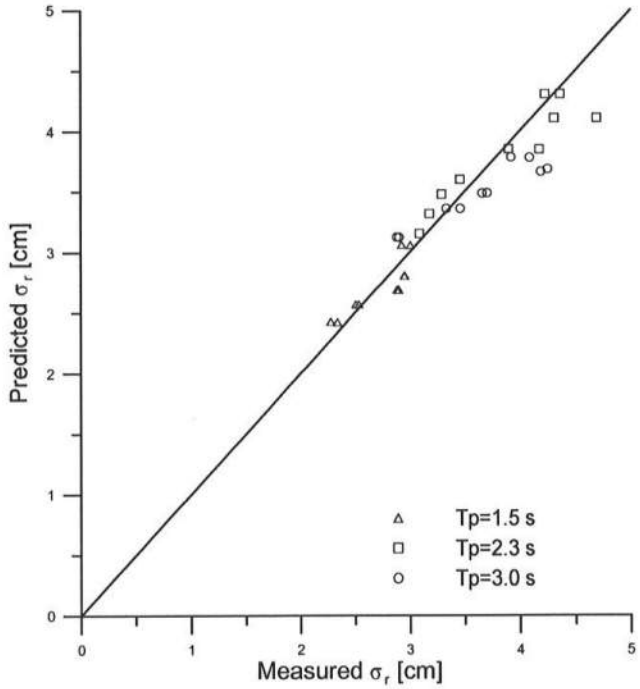

Fig. 5-26: Measured and predicted standard deviations of shoreline oscillations σ_r for 1/5 slope tests.

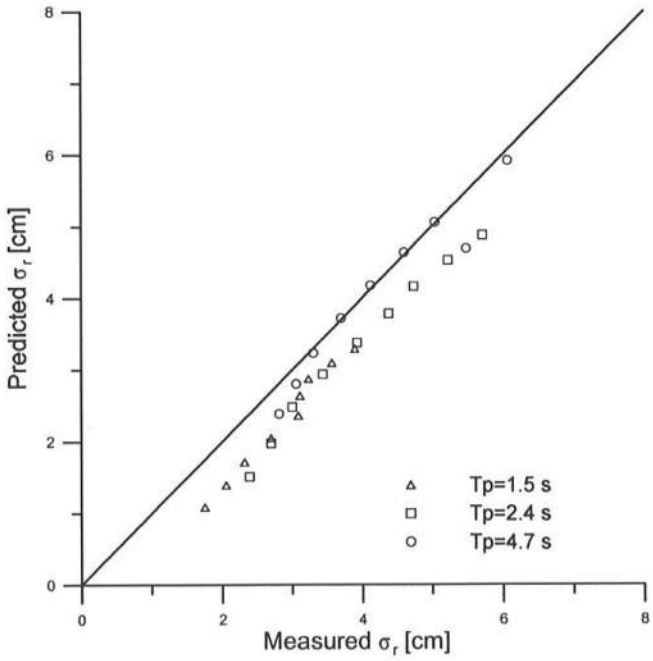

Fig. 5-27: Measured and predicted standard deviations of shoreline oscillations σ_r for 1/2 slope tests.

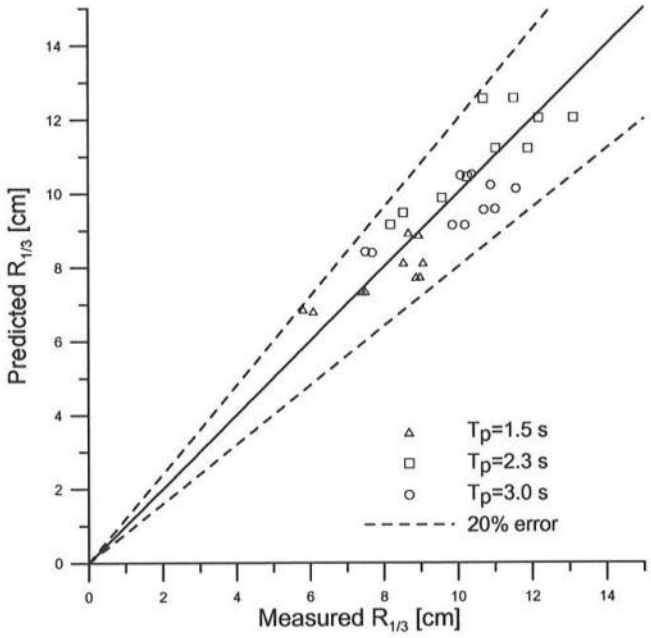

Fig. 5-28: Measured and predicted significant runup heights $R_{1/3}$ for 1/5 slope tests.

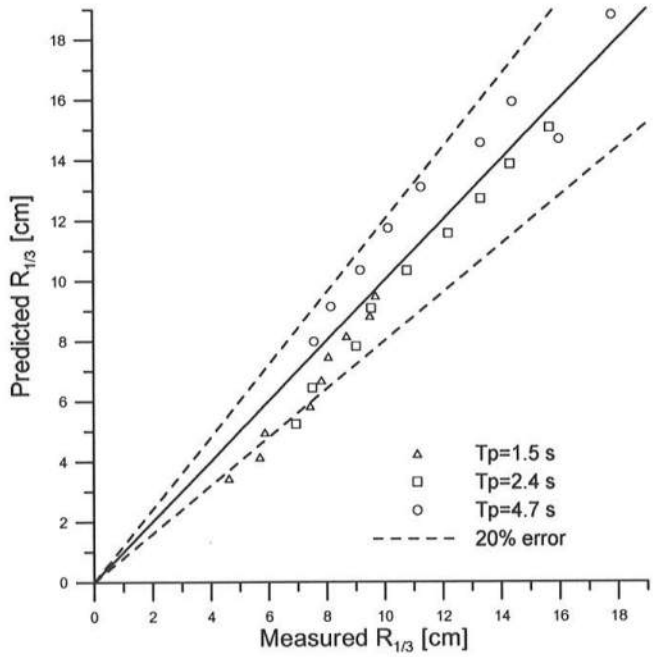

Fig. 5-29: Measured and predicted significant runup heights $R_{1/3}$ for 1/2 slope tests.

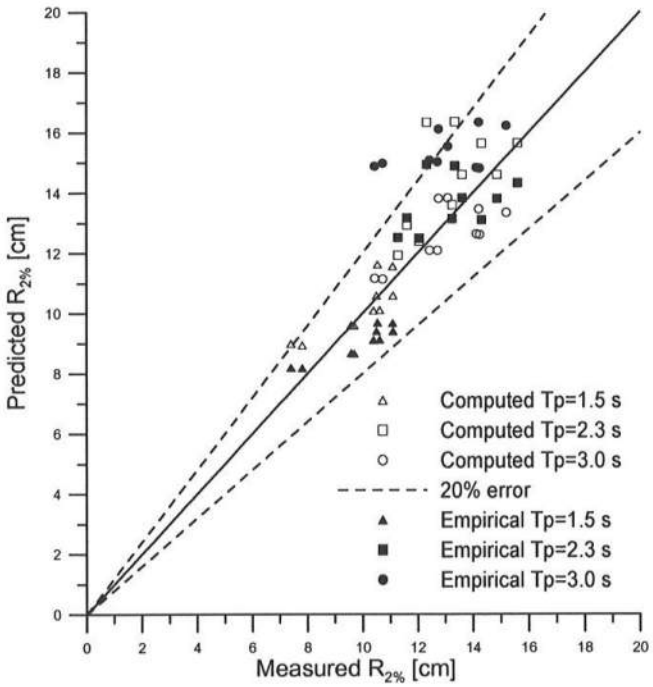

Fig. 5-30: Measured and predicted 2% runup heights $R_{2\%}$ for 1/5 slope tests.

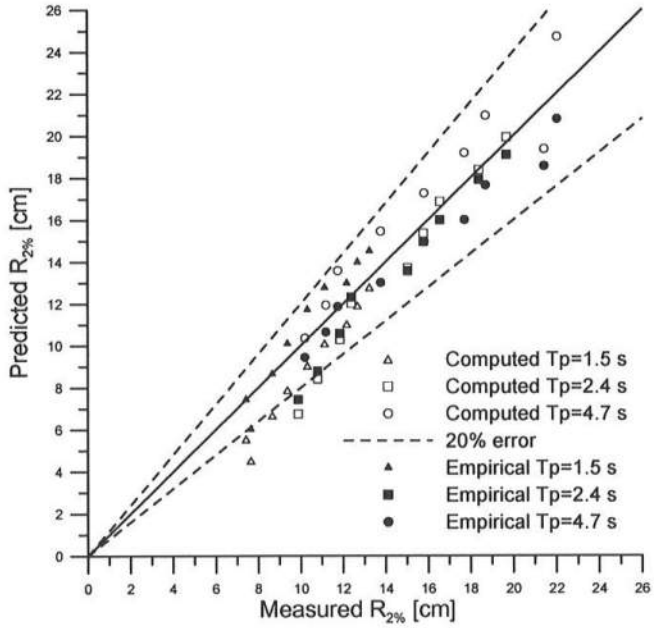

Fig. 5-31: Measured and predicted 2% runup heights $R_{2\%}$ for 1/2 slope tests.

Table 7: Comparison with empirical formula for 1/5 slope tests.

Test	d_t [cm]	T_p [s]	$H_{1/3}$ [cm]	ξ	γ_h	γ_f	γ_b	$\frac{R_{2\%}}{H_{1/3}}$	$R_{2\%}$ [cm]
R16A1	16.6	1.5	11.922	1.107	0.796	0.52	1	0.688	8.197
R18A1	18.6	1.5	13.248	1.050	0.798	0.52	1	0.654	8.660
R20A1	20.6	1.5	14.721	0.997	0.797	0.52	1	0.620	9.121
R22A1	22.6	1.5	15.052	0.986	0.813	0.52	1	0.625	9.404
R24A1	24.6	1.5	15.487	0.972	0.826	0.52	1	0.626	9.689
R16B1	16.6	2.3	12.536	1.630	0.785	0.52	1	0.999	12.518
R18B1	18.6	2.3	13.664	1.562	0.791	0.52	1	0.964	13.168
R20B1	20.6	2.3	15.020	1.490	0.793	0.52	1	0.921	13.834
R22B1	22.6	2.3	10.533	1.779	0.897	0.52	1	1.244	13.106
R24B1	24.6	2.3	17.045	1.398	0.804	0.52	1	0.877	14.944
R16C1	16.6	3.0	12.115	2.118	0.793	0.52	1	1.236	14.978
R18C1	18.6	3.0	11.714	2.154	0.825	0.52	1	1.288	15.084
R20C1	20.6	3.0	11.008	2.222	0.864	0.52	1	1.348	14.838
R22C1	22.6	3.0	12.029	2.126	0.865	0.52	1	1.349	16.233
R24C1	24.6	3.0	10.982	2.225	0.907	0.52	1	1.415	15.540

d_t =toe depth; T_p =peak period; $H_{1/3}$ =significant wave height at gauge 6 located at the toe of the porous slope; $\xi = \tan\theta / \sqrt{2\pi H_{1/3} / (gT_p^2)}$ = surf similarity parameter; g = acceleration due to gravity; γ_h = reduction factor due to a shallow foreshore; γ_f = reduction factor due to slope roughness; γ_b = reduction factor for a berm; $R_{2\%}$ = 2% runup level.

Table 8: Comparison with empirical formula for 1/2 slope tests.

Test	d_t [cm]	T_p [s]	$H_{1/3}$ [cm]	ξ	γ_h	γ_f	γ_b	$\frac{R_{2\%}}{H_{1/3}}$	$R_{2\%}$ [cm]
A4	4.0	4.7	9.898	9.333	0.612	0.52	1	0.955	9.452
A6	6.0	4.7	10.567	9.033	0.647	0.52	1	1.009	10.658
A8	8.0	4.7	11.276	8.745	0.675	0.52	1	1.053	11.876
A10	10.0	4.7	11.924	8.504	0.700	0.52	1	1.092	13.024
A12	12.0	4.7	13.536	7.981	0.709	0.52	1	1.106	14.975
A14	14.0	4.7	14.086	7.824	0.729	0.52	1	1.137	16.017
A16	16.0	4.7	15.359	7.493	0.737	0.52	1	1.150	17.669
A18	18.0	4.7	15.768	7.395	0.755	0.52	1	1.178	18.568
A20	20.0	4.7	17.721	6.975	0.753	0.52	1	1.174	20.806
B4	4.0	2.4	7.455	5.492	0.640	0.52	1	0.999	7.444
B6	6.0	2.4	8.321	5.198	0.677	0.52	1	1.057	8.794
B8	8.0	2.4	9.738	4.805	0.697	0.52	1	1.087	10.587
B10	10.0	2.4	11.089	4.503	0.712	0.52	1	1.111	12.317
B12	12.0	2.4	11.912	4.344	0.731	0.52	1	1.141	13.590
B14	14.0	2.4	12.865	4.180	0.746	0.52	1	1.163	14.965
B16	16.0	2.4	13.449	4.089	0.763	0.52	1	1.190	16.009
B18	18.0	2.4	15.042	3.866	0.764	0.52	1	1.192	17.933
B20	20.0	2.4	15.797	3.773	0.776	0.52	1	1.210	19.117
C4	4.0	1.5	5.747	3.909	0.673	0.52	1	1.049	6.030
C6	6.0	1.5	6.713	3.617	0.711	0.52	1	1.108	7.441
C8	8.0	1.5	7.474	3.428	0.743	0.52	1	1.158	8.657
C10	10.0	1.5	8.517	3.211	0.760	0.52	1	1.186	10.104
C12	12.0	1.5	9.772	2.998	0.769	0.52	1	1.200	11.730
C14	14.0	1.5	10.383	2.908	0.789	0.52	1	1.231	12.780
C16	16.0	1.5	10.097	2.949	0.825	0.52	1	1.287	12.994
C18	18.0	1.5	10.694	2.866	0.839	0.52	1	1.309	13.996
C20	20.0	1.5	10.818	2.849	0.861	0.52	1	1.343	14.533

d_t =toe depth; T_p =peak period; $H_{1/3}$ =significant wave height at gauge 9 located at the toe of the revetment; $\xi = \tan\theta / \sqrt{2\pi H_{1/3} / (gT_p^2)}$ = surf similarity parameter; g = acceleration due to gravity; γ_h = reduction factor due to a shallow foreshore; γ_f = reduction factor due to slope roughness; γ_b = reduction factor for a berm; $R_{2\%}$ = 2% runup level.

5.7 WAVE REFLECTION COEFFICIENT

Fig. 5-32 and Fig. 5-33 compare the measured and predicted reflection coefficient r at $x = 0$ for the 1/5 and 1/2 slope experiments, respectively, where r is predicted using Eq. (11). The numerical model overpredicts r for the 1/5 slope and underpredicts r for the 1/2 slope. The error is of the order of 30%. The wave reflection coefficient estimated from the residual wave energy flux at the still water shoreline may be crude but is useful in estimating the order of magnitude of wave reflection using the time-averaged model.

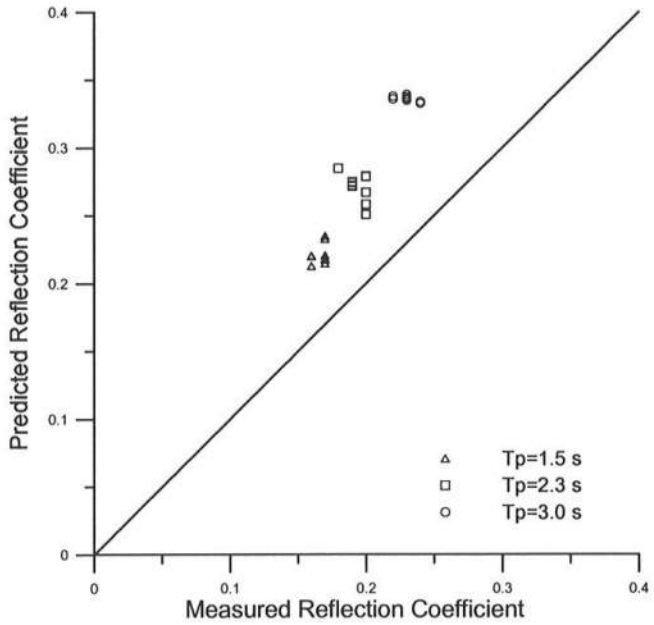

Fig. 5-32: Measured and predicted wave reflection coefficients r for 1/5 slope tests.

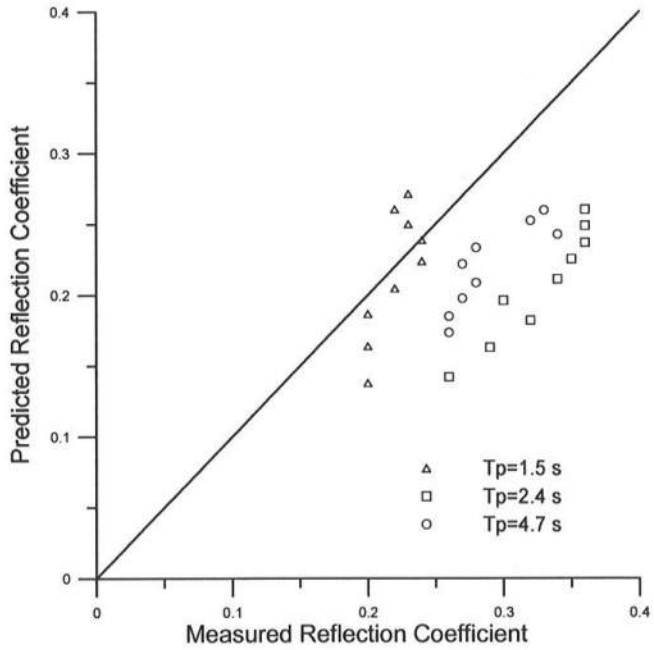

Fig. 5-33: Measured and predicted wave reflection coefficients r for 1/2 slope tests.

CHAPTER 6 CONCLUSIONS

The numerical model developed for the prediction of irregular breaking wave transmission over a submerged porous breakwater by Kobayashi et al. (2005) is extended to predict irregular wave shoaling and breaking on a beach with a gentle slope and irregular wave runup on a permeable slope that represents a cobble beach and a stone revetment. The numerical model based on the time-averaged continuity, momentum and energy equations predicts the cross-shore variations of the mean and standard deviation of the free surface elevation and the horizontal velocities above and inside the permeable layer. The mean and standard deviation of the shoreline oscillations on the permeable slope are estimated using the predicted statistics of the free surface elevation as shown in Fig. 2-2. The probability distribution of individual runup heights above SWL is assumed to be given by the Rayleigh distribution where the effect of wave setup is included. The significant runup height is related empirically to the mean and standard deviation of the shoreline oscillations.

The developed model is compared with the 1/5 slope experiment, described in Chapter 3, and the 1/2 slope experiment of Kearney and Kobayashi (2001). The numerical model is

shown to predict the cross-shore variations of the mean and standard deviation of the measured free surface elevation and horizontal velocity fairly accurately when the breaker ratio parameter γ is calibrated for some of the 1/2 slope tests. The computed results with and without the permeable layer are compared to examine the degree of the permeability effects which are found to reduce the wave energy dissipation rate due to wave breaking. Computations are also made to examine the sensitivities of the model to the bottom friction factor, the breaker ratio parameter and the roller volume flux. The numerical model predicts the mean and standard deviation of the measured shoreline oscillations reasonably well except that the mean is overpredicted for some of the 1/2 slope tests. Nevertheless, the numerical model predicts the significant and 2% runup heights within the error of about 20%. This accuracy is similar to the accuracy of available empirical formulas based on the known wave conditions at the toe of the permeable slope. The advantage of this numerical model is that it can predict the irregular wave transformation on a beach of arbitrary profile including a nearshore bar (Kobayashi et al. 2005). Furthermore, the numerical model may be applied to gentler permeable slopes for which the effect of wave setup is not negligible. This numerical model is computationally efficient and easy to use because no numerical difficulty has been experienced in the region of very small water depth.

REFERENCES

Abramowitz, M. and Stegun, I.A. (1972). *Handbook of mathematical functions*. Dover, New York, N.Y.

Battjes, J.A., and Stive, M.J.F., (1985). "Calibration and verification of a dissipation model for random breaking waves." *J. Geophys. Res.*, 90(C5), 9159-9167.

Deigaard, R. (1993). "A note on the three dimensional shear stress distribution in a surf zone." *Coastal Eng.*, 20, 157-171.

Goda, Y. (2000). *Random seas and design of maritime structures.* World Scientific, Singapore.

Gran, S. (1992). *A course in ocean engineering*. Elsevier, New York, N.Y.

de los Santos, F.J., Kobayashi, N., Meigs, L.E., and Losada, M.A. (2005). "Irregular wave runup on porous structures and cobble beaches." *Proc. Waves'2005 Conf.*, ASCE, Madrid, Spain. (in press).

Johnson, B.D., and Kobayashi, N. (1998). "Nonlinear time-averaged model in surf and swash zones." *Coastal Engineering 1998, Proc. 26th Coastal Engineering Conf.*, ASCE, Reston, Va., 2785-2798.

Kearney, P.G., and Kobayashi, N. (2000). "Time-averaged probabilistic model for irregular wave runup on coastal structures." *Coastal Engineering 2000, Proc. 27th Coastal Engineering Conf.*, ASCE, Reston, Va., 2004-2017.

Kearney, P.G., and Kobayashi, N. (2001). "Irregular breaking wave transformation on a beach and runup on a revetment." *Research Rep. No. CACR-01-01*, Center for Applied Coastal Research, Univ. of Delaware, Newark, Del.

Kobayashi, N. (1999). "Wave runup and overtopping on beaches and coastal structures." *Advances in Coastal and Ocean Engineering*, World Scientific, Singapore, 5,95-154.

Kobayashi, N., Cox, D.T., and Wurjanto, A. (1990). "Irregular wave reflection and run-up on rough impermeable slopes." *J. Waterw., Port, Coastal, Ocean Eng.*, 116(6), 708-726.

Kobayashi, N., de los Santos, F.J., and Kearney, P.G. (2005). "Time-averaged probabilistic model for irregular wave runup on permeable slopes." *J. Waterw., Port, Coastal, Ocean Eng.*, (submitted).

Kobayashi, N., Herrman, M.N., Johnson, B.D., and Orzech, M.D. (1998). "Probability distribution of surface elevation in surf and swash zones." *J. Waterw., Port, Coastal, Ocean Eng.*, 124(3), 99-107.

Kobayashi, N., Meigs, L.E., Ota, T., and Melby, J.A. (2005). "Irregular breaking wave transmission over submerged porous breakwater." *J. Waterw., Port, Coastal, Ocean Eng.* (in press).

Kobayashi, N., Otta, A.K., and Roy, I. (1987). "Wave reflection and runup on rough slopes." *J. Waterw., Port, Coastal, Ocean Eng.*, 113(3), 282-298.

Kobayashi, N., Zhao, H., and Tega, Y. (2005). "Suspended sand transport in surf zones." *J. Geophys. Res.* (in press).

Liu, P.L.-F., Lin, P., Chang, K.-A., and Sakakiyama, T. (1999). "Numerical modeling of wave interaction with porous structures." *J. Waterw., Port, Coastal, Ocean Eng.*, 125(6), 322-330.

Orzech, M.D., and Kobayashi, N. (1997). "Random wave transformation and sediment transport across barred and terraced sand beaches" *Research Rep. No. CACR-97-06*, Center for Applied Coastal Research, Univ. of Delaware, Newark, Del.

Stive, M.J.F., and DeVriend, H.J. (1994). "Shear stresses and mean flow in shoaling and breaking waves." *Coastal Engineering 1994, Proc. 24th Coastal Engineering Conf.*, ASCE.

Svendsen, I.A.. (1984). "Mass flux and undertow in a surf zone." *Coastal Eng.*, 8, 347-365.

Tayfun, M.A.(2004). "Statistics of wave crests in storms." *J. Waterw., Port, Coastal, Ocean Eng.*, 130(4), 155-161.

van der Meer, J.A., and Janssen, P.F.M. (1995). "Wave run-up and wave overtopping at dikes." *Wave forces on inclined and vertical wall structures,* ASCE. Reston, Va., 1-27.

van der Meer, J.A., Petit, H.A.H., van der Bosch, P., Klopman, G., and Broekens, R. (1992). "Numerical simulation of wave motion on and in coastal structures." *Coastal Engineering 1992, Proc. 23rd Coastal Engineering Conf.,* Reston, Va., 1772-1784.

van Gent, M.R.A. (1995). "Porous flow through rubble-mound materials." *J. Waterw., Port, Coastal, Ocean Eng.*, 121(3), 176-181.

van Gent, M.R.A. (2001). "Wave runup on dikes with shallow foreshores." *J. Waterw., Port, Coastal, Ocean Eng.*, 127(5), 254-262.

Wurjanto, A., and Kobayashi, N. (1993). "Irregular wave reflection and runup on permeable slopes." *J. Waterw., Port, Coastal, Ocean Eng.*, 119(5), 537-557.